

A High Statistic Search for Ultra-High Energy Gamma-Ray Emission from Cygnus X-3 and Hercules X-1

A. Borione, M.C. Chantell, C.E. Covault, J.W. Cronin, B.E. Fick, J.W. Fowler, L.F. Forston, K.G. Gibbs, K.D. Green, B.J. Newport, R.A. Ong, S. Oser, L.J. Rosenberg*
The Enrico Fermi Institute, The University of Chicago, Chicago, IL 60637, USA

M.A. Catanese[†], M.A.K. Glasmacher, J. Matthews, D. Sinclair, J.C. van der Velde
Department of Physics, The University of Michigan, Ann Arbor, MI 48109, USA

D.B. Kieda
Department of Physics, The University of Utah, Salt Lake City, UT 84112, USA

(To be published in Physical Review D)

Abstract

We have carried out a high statistics (2×10^9 events) search for ultra-high energy gamma-ray emission from the X-ray binary sources Cygnus X-3 and Hercules X-1. Using data taken with the CASA-MIA detector over a five year period (1990-1995), we find no evidence for steady emission from either source. The derived 90% c.l. upper limit to the steady integral flux of gamma-rays from Cygnus X-3 is $\Phi(E > 115 \text{ TeV}) < 6.3 \times 10^{-15}$ photons $\text{cm}^{-2} \text{sec}^{-1}$, and from Hercules X-1 it is $\Phi(E > 115 \text{ TeV}) < 8.5 \times 10^{-15}$ photons $\text{cm}^{-2} \text{sec}^{-1}$. These limits are more than two orders of magnitude lower than earlier claimed detections and are better than recent experiments operating in the same energy range. We have also searched for transient emission on time periods of one day and 0.5 hr and find no evidence for such emission from either source. The typical daily limit on the integral gamma-ray flux from Cygnus X-3 or Hercules X-1 is $\Phi_{\text{daily}}(E > 115 \text{ TeV}) < 2.0 \times 10^{-13}$ photons $\text{cm}^{-2} \text{sec}^{-1}$. For Cygnus X-3, we see no evidence for emission correlated with the 4.8 hr X-ray periodicity or with the occurrence of large radio flares. Unless one postulates that these sources were very active earlier and are now dormant, the limits presented here put into question the earlier results, and highlight the difficulties that possible future experiments will have in detecting gamma-ray signals at ultra-high energies.

1 Introduction

Cosmic ray particles span a remarkable range of energies, from the MeV scale to more than 10^{20} eV (eV = electron Volt). At energies above 1 TeV (10^{12} eV), we know that cosmic rays do not originate from local sources in or nearby our Solar System. Therefore, high energy cosmic rays must come from acceleration sites in the Galaxy at large or from outside the Galaxy. Remarkably, after many years of research, the exact sites of high energy cosmic ray acceleration remain unknown.

There are several difficulties that plague efforts to pinpoint the origins of high energy cosmic rays. First, since the bulk of the cosmic radiation is electrically charged, any source information contained in the directions of the arriving particles is lost due to deflection in the Galactic magnetic field. A second difficulty concerns the energetics of the proposed cosmic ray acceleration

mechanisms. For example, although models based on shock acceleration in supernova remnants offer plausible explanations for the cosmic ray origin up to 10^{14} eV (and perhaps up to 10^{15} eV), these models become less satisfying and less realistic at energies above 10^{15} eV. Since cosmic ray origins remain mysterious, it is natural to search for neutral radiation from point sources which, if seen, could pinpoint possible acceleration sites. The question of cosmic ray origin is thus a prime motivation for high energy neutral particle (gamma-ray or neutrino) astronomy.

In addition to supernova remnants, possible galactic sources of high energy particles include pulsars and compact binary systems. Gamma-radiation has been unambiguously detected from the Crab Nebula (a supernova remnant) at energies up to 10 TeV by ground-based detectors [1], but, historically, the compact binary sources Cygnus X-3 and Hercules X-1 have received considerably greater attention in the ground-based astronomical community. In the period 1975-1990, literally dozens of gamma-ray detections from Cygnus X-3 and Hercules X-1 were reported by numerous experiments. The detections spanned a wide range of energies (100 MeV to 10^{17} eV) [2], were generally of low statistical significance (typically three to four standard deviations), and episodic in nature. Often a statistically significant signal could only be extracted as a result of a periodicity analysis, where the data were phase-locked to a known source X-ray periodicity. In spite of these difficulties, the sheer number of reports made it difficult to dismiss the detections as being entirely due to statistical fluctuation [3]. In fact, by the late 1980's, it was generally established that Cygnus X-3 and Hercules X-1 were powerful emitters of high energy gamma-rays (although contrary interpretations of the data existed [4]). A number of new, more sensitive ground-based air shower arrays were commissioned at this time, including the CASA-MIA experiment in Dugway, Utah (USA). This paper describes long-term (1990-1995) observations of Cygnus X-3 and Hercules X-1 by CASA-MIA.

In the following section, we outline the experimental techniques of gamma-ray astronomy. We summarize the properties of Cygnus X-3 and Hercules X-1, and review previous observations of these sources and the astrophysical ramifications from the observations. We then turn our attention to the experimental apparatus, the event reconstruction procedures, and the methods used to select gamma-ray candidate events. We present results from a data sample of 2×10^9 events, and conclude with comparisons of our results to those of earlier and contemporaneous experiments.

2 Experimental Techniques of Gamma-Ray Astronomy

Gamma-ray sources typically exhibit power law spectra; fluxes fall rapidly with increasing energy. Space-borne experiments (on satellites or balloons) currently have sufficient sensitivity to detect gamma-rays up to an energy of ~ 10 GeV. Astronomy at higher energies requires very large collection areas available only to ground-based telescopes. Ground-based instruments rely upon the fact that high energy gamma-rays interact in the Earth's atmosphere to produce extensive air showers. At energies near 1 TeV, atmospheric Cherenkov telescopes use optical techniques to detect the Cherenkov radiation in the shower. At higher energies (~ 10 TeV and above), the charged particles in the shower penetrate to ground level. Here, air shower arrays record the arrival times and particle densities of the charged particles. At energies above 10^{17} eV, there is enough energy in the shower to allow the detection of nitrogen fluorescence in the atmosphere. The faint near ultraviolet fluorescence signal can be optically detected at night by experiments such as the Fly's Eye.

3 Discussion of the Sources and Earlier Results

3.1 Cygnus X-3

Cygnus X-3 is one of the most luminous X-ray sources in our Galaxy [5]. The X-ray emission is characterized by a 4.8 hr periodicity, which is assumed to be associated with the orbital motion of a compact object (neutron star or black hole) around its binary companion. The periodicity has been well studied; a complete ephemeris is available for the period from 1970-1995 [6, 7, 8, 9]. In addition to being a powerful X-ray source, Cygnus X-3 is seen in the infrared and is a strong and variable radio source. Radio flares have been detected in which the output from the source increases by two to three orders of magnitude on the time scale of days [10, 11, 12, 13]. These flares were first detected in 1972 and the outbursts have continued through 1994. Since Cygnus X-3 lies in the galactic plane, its optical emission is largely obscured by interstellar material. The lack of a strong optical signal makes determination of the distance to Cygnus X-3 difficult, but general consensus places it near 10 kpc [14].

The first published result claiming the detection of gamma-ray emission from Cygnus X-3 came in 1977 from the SAS-2 satellite at low gamma-ray energies ($E > 35$ MeV) [15]. This result made use of an apparent correlation between the gamma-ray arrival times and the 4.8 hr X-ray periodicity. Later observations by the COS-B satellite [16] with a much larger source exposure failed to confirm the SAS-2 result, and the COS-B authors argued that the initial detection [15] was flawed because of an incorrect treatment of the diffuse gamma-ray component [17]. To complicate matters, there have been re-examinations of both the SAS-2 [18] and COS-B [19] data sets which claim that signals indeed exist in both cases. Most recently, the EGRET experiment on the Compton Gamma-Ray Observatory (CGRO) failed to detect gamma-ray emission from Cygnus X-3 at a sensitivity level comparable to COS-B [20]. To summarize, there exists some controversy as to whether low energy gamma-rays have *ever* been detected from Cygnus X-3. Regardless, it can be reasonably concluded that the source is not a strong emitter of gamma-rays in the energy range between 30 MeV and 10 GeV.

The first published report of very-high energy gamma-ray emission from Cygnus X-3 came from the Crimean Observatory using an atmospheric Cherenkov telescope at energies above 2 TeV [21]. This result was based on data taken between 1972 and 1977 and the emission was claimed to be correlated with the 4.8 hr X-ray period. From 1980 to 1990, there were numerous additional detections of Cygnus X-3 by atmospheric Cherenkov telescopes [22, 23, 24, 25, 26, 27, 28]. The detections were generally episodic in nature and usually required the use of the 4.8 hr periodicity to extract a signal. Evidence for a 12.6 msec gamma-ray pulsar inside the Cygnus X-3 system was claimed on more than one occasion [26, 28, 29].

At the higher energies accessible by ground arrays, evidence for ultra-high energy gamma-ray emission from Cygnus X-3 was presented by the Kiel array [30] and subsequently by the Haverah Park experiment [31]. These results were based on data taken between 1976 and 1980. The gamma-ray emission was apparently steady over this time period and was correlated with the X-ray periodicity. Additional evidence for gamma-ray emission from Cygnus X-3 was later reported by other air shower detectors [32, 33, 34, 35, 36].

At extremely-high energies ($E > 5 \times 10^{17}$ eV), evidence was presented for neutral particles from the direction of Cygnus X-3 by the Fly's Eye [37] and by Akeno [38] groups, based on data taken during the periods 1981-1989 and 1984-1989, respectively. These data apparently indicated steady emission of neutral particles from Cygnus X-3 that was uncorrelated with the X-ray periodicity. The Haverah Park experiment, operating in the same energy range, and during much of the same period in time, found no evidence for such emission [39].

The evidence from ground-based experiments for gamma-ray emission from Cygnus X-3 from 1975 to 1990 is shown in Figure 1. Here, the integral gamma-ray fluxes are plotted as a function of energy. Also shown is a single power law fit of the form $E^{-1.1}$. The fact that the gamma-ray fluxes at widely varying energies could be approximately fit by a single power law was taken by some as evidence of a unified acceleration mechanism at the source. One should note, however, that all results shown in Figure 1 represent *integral* flux measurements by experiments incapable of accurately measuring differential fluxes. Since the detections were generally only marginally statistically significant, the reported fluxes equally represent the three to four standard deviation sensitivity of each instrument at a fixed energy. The fluxes therefore would naturally fall on an E^{-1} power law, if the sensitivities of the experiments scaled linearly with energy (which was approximately true for these first-generation experiments). It has also been pointed out that even if the source mechanism produced emission with a single power law form, the *detected* flux at Earth would have a significant dip between 10^3 and 10^4 TeV because of absorption of gamma-rays by the cosmic microwave radiation [40].

Starting with the CYGNUS experiment in 1988 [41], a number of more sensitive ground-based experiments were unable to detect gamma-ray emission from Cygnus X-3, at levels significantly lower than the earlier reports. Upper limits on the flux were reported for experiments using both the atmospheric Cherenkov technique [42], as well as the ground-array technique [43, 44]. Using parts of the eventual CASA-MIA detector, some of us reported limits for data taken in 1988-1989 [45] and in 1989 [46]. The general trend of a “quiet” Cygnus X-3 continued into the early 1990’s, although there were several publications claiming gamma-ray emission based largely on data that had been taken in the previous decade [47, 48, 49].

3.2 Hercules X-1

Like Cygnus X-3, Hercules X-1 is a powerful binary X-ray source [50]. The X-ray emission is modulated on a time scale of 1.7 days which is assumed to result from the orbital motion of the binary pair. Unlike Cygnus X-3, Hercules X-1 is not seen in radio, but has been observed for many years in the optical range [51] and a 5.8 kpc distance to the source has been determined [52]. In addition, Hercules X-1 contains an X-ray pulsar with a period of 1.24 sec [50], but whose ephemeris is relatively poorly determined because of unpredictable variations in the spin-up rate [53]. Hercules X-1 has not been detected by space-borne gamma-ray instruments.

The first evidence from a ground-based observatory for gamma-ray emission from Hercules X-1 was reported in 1984 by the Durham group using the atmospheric Cherenkov technique [54]. The reported gamma-ray emission came in the form of a short burst (~ 3 minute duration) that exhibited 1.24 sec periodicity. Following this report, additional pulsed emission was claimed by Cherenkov detectors operating at ultra-high energies ($E > 500$ TeV) [55] and at TeV energies [56, 57].

The most intriguing evidence for gamma-ray emission from Hercules X-1 came from data taken in 1986 by three experiments. Data taken between April and July of 1986 by the Haleakala [58] and Whipple [59] telescopes operating near 1 TeV, and by the CYGNUS experiment [60] in July of 1986 operating at energies above 50 TeV, all indicated evidence for gamma-ray emission from Hercules X-1 in the form of short bursts of approximately 0.5 hr duration. In addition, the emission detected by each experiment exhibited a common periodicity near 1.2358 sec, which differed by a significant amount ($\sim 0.16\%$ lower) from the known X-ray period. The data from the CYGNUS experiment was further puzzling because the events from the direction of Hercules X-1 had a muon content that was similar to the cosmic ray background events, whereas gamma-ray events should have contained significantly fewer muons. Later, two groups with somewhat poorer

sensitivity presented additional evidence for gamma-ray emission from Hercules X-1 at different times in 1986 at TeV [61] and 100 TeV [62] energies.

Since the advent of upgraded and improved experiments in the early 1990's, the gamma-ray signals from Hercules X-1 disappeared from the published literature. The Whipple group, using a more sensitive Cherenkov imaging technique, failed to detect emission from Hercules X-1, and found no statistically significant evidence for gamma-ray emission from Hercules X-1 over a six year period, even including their data from 1986 [63]. An enlarged and improved CYGNUS experiment also failed to see gamma-rays from Hercules X-1 in the period between 1987 and 1991 [64]. Using data taken in 1989, we reported upper limits on the emission of gamma-rays from Hercules X-1 using part of the eventual CASA-MIA experiment [46].

3.3 Theoretical Implications

The many claims of very high energy gamma-ray emission from the binary systems Cygnus X-3 and Hercules X-1 fueled great interest in the development of astrophysical models to explain such emission. There were also non-standard particle physics models put forward to explain the observations; these models will not be discussed here.

For the case of Cygnus X-3, where the gamma-ray emission was generally observed with a 4.8 hr periodicity, the astrophysical models needed to incorporate the orbital dynamics of the binary system. Models in which an energetic pulsar alone served as the power source for the gamma-rays [65] or in which accretion powered the gamma-rays [66] were proposed. These models generally had difficulty in producing gamma-rays at energies above 10^{15} eV. More popular were a general class of models in which the gamma-rays were produced from the decays of π^0 mesons made in hadronic collisions [67, 68, 69]. The hadronic beam resulted from diffusive shock acceleration, perhaps near the neutron star, and possible beam targets included the atmosphere of the companion star or material in the accretion disk. Such “beam-dump” models were capable of explaining gamma-rays at ultra-high energies and were also able to accommodate the observed periodicities of the gamma-ray signals. Several authors recognized that in order to explain the ultra-high energy gamma-ray fluxes initially seen, the required luminosity of Cygnus X-3 would also be sufficient to account for a substantial fraction of the high energy cosmic ray flux [70]. Hillas pointed out that if Cygnus X-3 consisted of a 10^{17} eV accelerator with a luminosity of $\sim 10^{39}$ ergs/sec, only one such object like it would be required to explain the origin of cosmic rays above 10^{16} eV [71].

Unlike Cygnus X-3, the gamma-ray emission from Hercules X-1 was not seen to be correlated with the orbital motion of the binary system, but instead with the pulsar periodicity. This observation, along with evidence that the emission appeared in the form of short bursts, led naturally to models in which the pulsar itself was the power source. In such models, the gamma-rays were produced by the interaction of a charged particle beam with the accretion disk [72, 73]. More difficult to explain were the 1986 observations of gamma-ray emission at a slightly shorter period than the X-ray period. The anomalous gamma-ray periodicity was explained by the presence of matter in the accretion disk which periodically obscured the gamma-ray interaction region [74, 75].

In summary, although theoretical difficulties existed in explaining the apparent signals of gamma-rays from Cygnus X-3 and Hercules X-1, the signals were tantalizing because of the possibility that they revealed important sources of the ultra-high energy cosmic ray flux.

4 Experimental Procedure

Table 1: Size and makeup of CASA-MIA experiment as a function of time for the data sample used in this analysis. A range of values indicates that the experiment was being enlarged during this period of time. Data taken after August 1995 are not used in this analysis.

| Epoch | Enclosed Area (m ²) | CASA Detectors | MIA Counters |
|-----------------------|---------------------------------|----------------|--------------|
| Mar. 1990 – Oct. 1990 | 108,900 | 529 | 512 |
| Oct. 1990 – Apr. 1991 | 108,900–230,400 | 529–1089 | 512–1024 |
| Jan. 1992 – Aug. 1993 | 230,400 | 1089 | 1024 |
| Aug. 1993 – Aug. 1995 | 216,225 | 1056 | 1024 |

4.1 The CASA-MIA Experiment

The CASA-MIA experiment is located in Dugway, Utah, USA (40.2° N, 112.8° W) at an altitude of 1450 m above sea level (870 g/cm² atmospheric depth). CASA-MIA consists of two major components: the Chicago Air Shower Array (CASA), a large surface array of scintillation detectors, and the Michigan Array (MIA), a buried array of scintillation counters sensitive to the muonic component of air showers.

CASA consists of 1089 scintillation detectors placed on a 15 m square grid and enclosing an area of 230,400 m². Construction on the array started in 1988 and a small portion (5%) of the experiment operated in 1989. A more substantial portion (~50%) of it was completed by early 1990. Data collection with this portion started on March 1, 1990. Additional detectors were added in 1990 to complete the construction.

MIA consists of 1024 scintillation counters located beneath CASA in 16 groupings (patches). The total active scintillator area is 2,500 m² and the counters are buried beneath ~ 3.5 m of soil. This depth corresponds to a muon threshold energy of approximately 0.8 GeV. Parts of MIA were operational as early as 1987, 50% of the experiment was completed by early 1990, and the entire array was working by early 1991. The CASA-MIA experiment was turned off temporarily in 1991 for repair due to lightning damage, but has operated essentially uninterrupted since that time. Table 1 summarizes the size and detector makeup of CASA-MIA as a function of time.

Figure 2 shows a plan view of the experimental site. In addition to CASA-MIA, there are other installations at the same site. The other equipment used in this analysis is an array of five tracking Cherenkov telescopes. One telescope is located at the center of CASA-MIA, and the other four are 120 m away from the center along the major axes. Each telescope consists of a 35 cm diameter mirror which focuses Cherenkov radiation onto a single 5.1 cm photomultiplier tube (PMT). The signals from the PMTs are digitized to record the amplitude and time of arrival of the Cherenkov wavefront at each telescope location. The shower direction is reconstructed by fitting the Cherenkov arrival times to a conical wavefront.

A complete description of the CASA-MIA experiment can be found elsewhere [76]; here we briefly describe some aspects of the experiment that are relevant for this analysis. Each CASA station consists of four scintillation counters connected to a local electronics board. A station is *alerted* when at least two of the four counters fire within a 30 nsec window and it is *triggered* when at least three of the counters fire. If three or more stations trigger within a time period of approximately 3 μ sec, an *array trigger* is said to have occurred. The array trigger rate depends on operating conditions (e.g. atmospheric pressure), but is ~20 Hz for the full CASA-MIA experiment.

Upon an array trigger, the Universal Time (UT) is latched and recorded by either a GOES

Satellite Receiver Clock (1990-1993) with a precision of ± 1 msec, or by a Global Positioning System (GPS) clock (1993-1995) with a precision of ± 100 nsec. For each array trigger, a command is broadcast to the array instructing each alerted CASA station to digitize and record its data, and a signal is generated to stop time-to-digital converters (TDCs) on each MIA counter. The TDCs have a range of $4 \mu\text{sec}$ and a least bit precision of 4 nsec. The data from each CASA station consist of the arrival times and pulse-height amplitudes of the pulses from each scintillation counter, as well as the arrival times of pulses from the four nearest neighbor stations. The data from each MIA counter consist of the time of arrival of the array trigger relative to the passage of a muon through the counter. The CASA-MIA data and the Universal Time recorded as the result of an array trigger correspond to a single air shower *event*.

4.2 Event Reconstruction

We briefly summarize some of the important aspects of the CASA-MIA event reconstruction; full details can be found elsewhere [76]. The data from the experiment are accumulated in runs of six hours duration. All calibrations and offsets are determined for each run separately. At the start of a run, the timing constants associated with the CASA station electronics are calibrated by an internal oscillator. Timing constants are corrected for the effects of temperature by studying the constants over the span of a week. The CASA counter particle gains are determined for each run from the abundant cosmic ray air showers. The counter gains are found from the PMT amplitude distributions of those counters hit in stations with two out of four counters hit. A statistical correction of $\sim 20\%$ accounts for the fact that on average slightly more than one particle passes through a counter in this situation. The CASA cable and electronic delays are determined from the zenith angle distributions of the detected events. The relative delay between the CASA and MIA trigger systems is determined by centering the peak of the muon arrival time distribution relative to the position of the CASA trigger time.

We estimate the shower *core position* by the location on the ground with the highest particle density. The total number of particles in the shower, or *shower size*, is determined by fitting the density samples obtained from the CASA stations to a lateral distribution of fixed form. The mean number of alerted CASA stations is 19 and the mean shower size is $\sim 25,000$ equivalent minimum ionizing particles.

The *shower direction* is determined from the timing information recorded by CASA. The relative times between pairs of adjacent alerted CASA stations are determined. Each relative time gives a measure of the shower direction along one axis of the experiment. The times are weighted by an empirical function of the local particle density and distance to the shower core, and are fit to a wavefront which accounts for the conical shape of the shower front. The cone slope is approximately 0.07 nsec/m . The shower direction in local coordinates is defined by two angles. The zenith angle, θ , is measured with respect to the vertical direction and the azimuthal angle, ϕ , is measured with respect to East in a counter-clockwise manner.

In order to be confident of any astronomical results, it is essential to measure the *angular resolution* of the experiment. The resolution has two parts. The statistical part largely derives from the intrinsic fluctuations in the arrival times of the shower particles and from the timing resolution of the CASA counters and electronics. The systematic contribution derives primarily from the accuracies of the experiment survey and of the calculation of timing delays and offsets.

The statistical contribution to the angular resolution is determined by three different techniques. First, on an event-by-event basis, we divide the array into two overlapping sub-arrays and compare the shower directions that are reconstructed by each sub-array. Using an air shower and detector simulation, we estimate the statistical correction required to derive the angular res-

olution from the sub-array direction comparison. Second, we compare the shower direction as determined by CASA with the direction determined by the five Cherenkov telescopes for events in which both CASA and the telescopes triggered. By statistically removing the angular resolution of the telescopes from this comparison, we estimate the CASA resolution. Third, we have detected the shadow that the Moon casts in the cosmic rays [77]. For data taken between 1990 and 1995, the Moon shadow is shown in Figure 3. By deconvolving the size of the Moon from the measured shadow, we obtain another estimate of the angular resolution. Figure 4 shows the resolution estimates from these different techniques. The agreement between the various methods is good, which allows us to determine a single parametric form for the resolution as a function of the number of alerted CASA stations.

The systematic contribution to the angular resolution of the experiment has been checked by two different techniques. First, for data taken in coincidence with the tracking Cherenkov telescopes, we examine the angular difference between the directions determined by CASA and by the telescopes. The distribution of these differences indicates that the systematic offset between CASA and the telescope array is very small ($< 0.1^\circ$). The alignment of the telescope array has been verified by the observation of a number of stars. A second check on the pointing accuracy of CASA comes from the Moon shadow. The center of the Moon shadow image is within 0.1° of the known position of the Moon. We conclude that the pointing uncertainty of CASA is negligible in comparison with the experiment's angular resolution.

The *muon content* of the shower is determined from the data recorded by MIA. Since MIA records the times of counter hits over an interval of $4\mu\text{sec}$, it is sensitive to muons produced by showers arriving at any location of the array and from any direction. During the same time interval, MIA also records accidental counter hits produced by PMT noise and by natural radioactivity in the ground. The average number of accidental hits is approximately sixteen per event, while the average number of real muons associated with air showers is approximately nine per event.

Real muons arrive within 100 nsec of the shower front arrival, while the accidental hits occur randomly over the $4\mu\text{sec}$ interval. We greatly reduce the acceptance for accidental muon hits by narrowing the time window for accepting muons. The width of the window is determined from the distribution of muon times for each six hour run. We set the width to encompass 95% of the real shower muons; on average, it is ~ 150 nsec. The position of the window is found on an event-by-event basis by means of a clustering algorithm. The algorithm searches for the cluster of three or more muons within an interval of 40 nsec. In approximately 25% of the events, no cluster is found and the window position is placed at the center of the muon time distribution as determined for the entire run. As a result of tightening the time window for muon hit acceptance, the average number of real muons recorded is 8.5 per event, while the average number of accidentals is 0.63 per event.

The CASA-MIA data undergo several stages of processing and compression. In the most highly compressed format upon which this analysis is based, the data records are 26 Bytes per event and include the following information for each event: Universal Time (UT), number of alerted CASA stations, number of in-time muon hits, core location, arrival direction, shower size, and muon shower size (not used here).

5 Analysis

5.1 Data Sample

The data used in this analysis were taken between March 4, 1990 and August 10, 1995, with a gap of 255 days in 1991. The experiment had usable data on 1627 days with the remainder of the days

Table 2: Quality cut efficiencies and event totals for the CASA-MIA data sample. The muon-data quality cuts are applied after the all-data quality cuts. The data sets (all and muon) are described in the text.

| Category | All-Data Sample | Muon-Data Sample |
|----------------------|-----------------|------------------|
| Initial Event Total | 2087.8M | 1925.8M |
| Run Cut Efficiency | 0.935 | 0.929 |
| Event Cut Efficiency | 0.986 | 0.896 |
| Overall Efficiency | 0.922 | 0.832 |
| Final Event Total | 1925.8M | 1602.7M |

lost largely because of power outages at the site and computer problems. The experiment has an instrumental deadtime of approximately 5.4% which is due to a number of effects, including data acquisition computer latency and the time needed to digitize the CASA station data. Calibration runs of approximate length of six minutes taken at the start of data runs, losses due to 8 mm tape failures, and downtime from array maintenance led to an additional reduction in the live time to a total of 1378.4 days (84.7% of the total). After the reduction and processing of the data, the final data sample consisted of 2.0878×10^9 reconstructed events.

The size of the CASA-MIA data sample is unprecedented in air shower physics. To ensure data integrity, we impose a comprehensive set of data quality cuts. The cuts are tailored separately for the data sample in which we only use information from the surface array (*all-data*) and the sample in which we use information from both the surface and muon arrays (*muon-data*). For each of these samples, we make quality cuts on an event-by-event basis and on a run-by-run basis. Cuts are applied to runs and events only in the cases there there is evidence of an instrumental bias. The efficiencies of the cuts are summarized in Table 2.

For the all-data sample, the run and event cuts have a combined efficiency of 92.2%, which yields a final sample of 1.9258×10^9 events. The most restrictive run cut requires a minimum fraction of the CASA stations to be working reliably and removes 2.2% of the data, largely because of instances in which isolated parts of the array failed. For the muon-data sample, the run cuts have an efficiency of 92.9%. A cut which requires a sufficient fraction of the muon counters to be working removes 4.8% of the data. The event cuts have an additional efficiency of 89.6%. The most restrictive event cut eliminates 3.2% of the events because they have no muon information due to deadtime of the MIA data acquisition system. The overall efficiency of the muon-data cuts is 83.2%, which yields a final sample of 1.6027×10^9 events.

5.2 Gamma-Ray Selection

From prior observations of Cygnus X-3 and Hercules X-1, we expect that gamma-ray fluxes, if present, will be small in comparison with the isotropic cosmic ray flux. Therefore, we need to enhance the presence of a possible gamma-ray signal by eliminating as many cosmic ray air showers as possible, while keeping a high fraction of the gamma-ray air showers. To do this, we select those showers with a reconstructed direction consistent with the position of the sources (within the angular resolution of the experiment) and with a muon content consistent with that expected from a gamma-ray primary.

Table 3: Angular search bin sizes and event fractions as a function of the number of CASA alerts. The search bin is a circular region in equatorial coordinates whose radius is equal to 1.59 times the angular resolution.

| Alert Range | Event Fraction | Search Bin Radius |
|-------------|----------------|-------------------|
| 3 - 10 | 0.331 | 2.45° |
| 11 - 15 | 0.224 | 1.88° |
| 16 - 20 | 0.121 | 1.40° |
| 21 - 30 | 0.150 | 1.05° |
| 31 - 40 | 0.064 | 0.78° |
| 41 - 60 | 0.058 | 0.60° |
| > 60 | 0.052 | 0.41° |

5.2.1 Angular Search Bin

We define a circular search bin whose size is based on the estimated angular resolution of the experiment. For a sufficiently large number of events, the bin which optimizes the signal-to-noise has a size equal to 1.59 times the angular resolution and contains 72% of the signal. The CASA-MIA angular resolution depends on the number of alerted CASA stations in an event, and therefore we use a variable-sized search bin which scales with the number of alerts. For simplicity, we use seven different bin sizes that range from 2.45° radius for showers with the least number of alerts, to 0.41° radius for showers with the largest number of alerts. These bin sizes are shown in Table 3, along with the fraction of events in each alert range.

5.2.2 Muon Content

Air showers created by gamma-ray primaries are expected to contain far fewer muons than showers initiated by cosmic ray nuclei. This expectation results because the cross section for pion production is much smaller than the cross section for electron-positron pair production [78]. Therefore, the interaction of a high energy gamma-ray in the atmosphere is much more likely to produce an electromagnetic cascade in the atmosphere than it is to create a hadronic cascade. Conversely, cosmic ray nuclei preferentially interact to create hadronic cascades. Showers initiated by gamma-rays are thus expected to contain far fewer hadrons than those initiated by cosmic rays. Since air shower muons are predominantly produced from the decays of pions and kaons in the hadronic cascade, gamma-ray air showers should contain far fewer muons as well. Simulations have been done to estimate the muon content of air showers [79, 80]. Our own simulation indicates that an air shower initiated by a 100 TeV gamma-ray contains, on average, 3-4% of the number of muons in a shower initiated by a proton of the same energy.

The muon content of showers should in principle be a powerful tool in rejecting cosmic ray background events. In our experiment, the rejection capability is limited by the collection area of the muon array and, to a lesser extent, by the presence of a small amount of accidental muon hits. The muon array (MIA) is significantly larger than any other air shower muon detector built to date, but its active area still corresponds to only $\sim 1\%$ of the enclosed area of the experiment. As shown in Figure 5, the average of the distribution of the number of in-time muons is ~ 8.5 , but the shape of the distribution is such that its mode is three, and a substantial fraction of events have zero muons. In Figure 5, we also show the estimated number of muons for showers initiated

Table 4: Quantities associated with the selection of muon-poor events. Muon-poor events are those having a relative muon content, r_μ (defined in the text), less than a cut value. The cut values are given in the second column, and the third and fourth columns give the efficiencies for passing the cut for gamma-ray signal events and for hadronic background events, respectively. The fifth column gives the quality factor, Q, or the improvement in flux sensitivity from making the cut.

| Data Set | r_μ cut Value | Signal ϵ | Background ϵ | Q |
|------------------|-------------------|-------------------|-----------------------|------|
| All | -0.75 | 0.72 | 0.0600 | 2.94 |
| ≤ 10 Alerts | -0.50 | 0.69 | 0.1644 | 1.70 |
| > 10 Alerts | -0.75 | 0.76 | 0.0362 | 3.99 |
| > 40 Alerts | -1.00 | 0.71 | 1.77×10^{-3} | 16.9 |
| > 80 Alerts | -1.00 | 0.77 | 0.67×10^{-3} | 29.7 |

by gamma-rays, including the contribution from accidental muon hits. For gamma-ray showers, we expect, on average, 0.28 real muons per event and 0.63 accidental muons per event.

In order to enhance a possible gamma-ray signal, we wish to select *muon-poor* events, i.e. events that have fewer muons than the average expected number. To do this, we make the assumption that any gamma-ray signal in the data is much smaller than the flux of cosmic rays. We can therefore use the muon information from the detected events to describe the muon content of the background, and our simulation to describe the muon content of the gamma-ray signal.

The number of muons in a shower depends on a number of observable quantities, for example, the number of alerted CASA stations, shower zenith angle, and core position. We develop a parameterization for the average number of muons as a function of these quantities by examining a large ensemble of actual showers. We then determine the relative muon content of a specific shower by comparing the observed muon number, $(n_\mu)_{\text{obs}}$, to the expected number of muons, $\langle n_\mu \rangle_{\text{exp}}$, for showers having similar zenith angles, core positions, and numbers of alerts. The relative muon content, r_μ , is defined by:

$$r_\mu \equiv \text{Log}_{10} \left[\frac{(n_\mu)_{\text{obs}}}{\langle n_\mu \rangle_{\text{exp}}} \right]. \quad (1)$$

Figure 6 shows the distributions of r_μ for observed events and for simulated gamma-ray events. Muon-poor events are defined as those having r_μ values less than some cut value. The position of the cut is chosen to reject as many background events as possible, while keeping a high fraction of the gamma-ray events. The cut value depends weakly on the number of CASA alerts because the separation between the signal and background r_μ distributions improves as the showers get larger.

Table 4 shows the r_μ cut values for various samples of data along with the fractions of signal and background events retained, and the sensitivity improvement achieved from making a cut. For the entire data set, the sensitivity is improved by a factor of 2.94 by cutting on the shower muon content. The quality factor increases to 29.7 for events having more than 80 alerted CASA stations.

5.3 Background Estimation

We select gamma-ray candidate events (*on-source* events) based on their reconstructed arrival direction in equatorial coordinates (right ascension, α , and declination, δ) and on their muon content. In order to derive the significance of a possible gamma-ray signal, we need to determine the expected number of background cosmic ray events (*off-source* events) that would arrive from the same direction in the sky as the source and would have a similar muon content as gamma-ray events. Again, we make the assumption that the detected air showers are predominantly caused by background cosmic ray events. We thus use the detected events themselves to estimate the expected background.

A common method to estimate the expected number of background events is to use off-source bins having the same declination as the source, but having different right ascension values. This method, which assumes a uniform experiment exposure over declination, was satisfactory for earlier smaller experiments. However, given our large event sample, this technique is not reliable for CASA-MIA because of small, but non-negligible, systematic biases (e.g. diurnal variations). For the CASA-MIA data sample, a source at a declination of 40° occupies an angular bin with $\sim 1.8 \times 10^6$ events. The fractional statistical uncertainty corresponding to one standard deviation in the number of events is 0.075%. In order to accurately estimate the number of background events, the relative systematic uncertainty must be well below this level. As a result, an accurate and robust way to determine the expected background is needed. Several methods have been developed by other groups [37, 81] and the method that we use is similar to these.

The detection rate of an air shower array triggering on cosmic rays is determined by the properties of the cosmic ray flux and by the properties of the array itself. Assuming that the cosmic ray parameters do not change with time, any variation in the detection rate is caused only by changes in the detector or in the atmospheric conditions. Over short intervals of time (~ 1 hour), the relative detection efficiency as a function of the shower direction in local coordinates, (θ, ϕ) , is largely determined by the array geometry (placement of detectors, uniformity of terrain, etc.) and is almost constant, and the time variation of the detector response may be estimated from the trigger rate. Therefore, we separate the detection rate per unit solid angle in local coordinates, $N(\theta, \phi, t)$, into two terms:

$$N(\theta, \phi, t) = D(\theta, \phi) \cdot R(t) \quad , \quad (2)$$

where $D(\theta, \phi)$ is the efficiency per unit solid angle of detecting a shower from a given direction in the sky, and $R(t)$ is the trigger rate as a function of time. The factor $D(\theta, \phi)$ is determined by maps made from the arrival directions of cosmic ray showers over given periods of time. The time dependent term, $R(t)$, is determined from the arrival times of the actual events. The expected number of events for a given bin in the sky is then determined by integrating $N(\theta, \phi, t)$ over the time interval in question. To determine the expected number of events for a bin in equatorial coordinates, (α, δ) , we integrate $N(\theta, \phi, t)$ over the time interval and over local coordinate space.

More explicitly, the background estimation is done by the following procedure. For intervals of 4,200sec, we accumulate the arrival directions of cosmic ray events into 2,700 bins segmented in local coordinate space (30 bins in θ , 90 bins in ϕ). We use the binned data to construct maps of the relative acceptance of any point in the sky over this time interval. Separate maps are calculated for each data sample used in the source search (e.g. all-data and muon-poor data). To generate simulated background data, we discard the directional information of an event and associate the event time with a local coordinate direction obtained by sampling from the appropriate sky map. We then compute artificial values for the equatorial coordinates and determine if this simulated event falls into a search bin of a source. By sampling more than once from the sky map for each

event time, we increase the statistics on the simulated data sample. Negligible systematic bias is introduced by such oversampling. For this work, we oversample by a factor of ten, an amount that is limited only by computational resources.

We have checked that our background estimation method is free from bias by comparing the detected numbers of events in an angular bin to our expected number for bins that do not contain Cygnus X-3 and Hercules X-1. For each bin, we compute the statistical significance of any excess or deficit in the number of detected events relative to the number we predict. The distribution of these significances is in close agreement with that expected from statistics, which, because of background oversampling, is dominated by the statistical uncertainty on the number of detected events.

5.4 Energy Response

Air shower arrays trigger on the shower size, i.e. the number of charged particles in the shower at ground level. For each shower, we determine a shower size from the particle densities measured in the CASA stations. For astrophysical interpretations of flux measurements or flux limits, however, it is necessary to translate from the measured shower parameters (size and zenith angle) to an estimate of the energy of the primary particle. Since there are large fluctuations in shower size for showers initiated by particles at fixed energy, it is difficult for air shower experiments to measure accurately *differential* primary spectra. Traditionally, therefore, flux measurements have been quoted as *integral* intensities above a fixed energy point. Although to some degree the energy value at which to quote the intensity is arbitrary, we desire to use an energy at which the experiment has a significant degree of sensitivity. We chose to quote flux measurements at the *median* energy of the experiment which reduces the dependence of the flux on the assumed spectral index [45, 85].

We estimate the energy response of the experiment by the constant intensity method, which has been used by other experiments [82], as well as by our own group [83]. The constant intensity procedure is described in more detail elsewhere [84]. Briefly, we determine the relationship between shower size and energy by comparing the detected flux of showers above a given size to an assumed form of the all-particle cosmic ray spectrum. The comparison is done on a run-by-run basis to account for changes in the detector response. The cosmic ray flux is derived from measurements made by other space-borne [86, 87] and ground-based [82] experiments. The assumed integral cosmic ray intensity above 100 TeV is 6.57×10^{-9} particles $\text{cm}^{-2} \text{s}^{-1} \text{sr}^{-1}$.

We use the relationship between energy and shower size to determine the most likely energy for each shower coming from the direction of Cygnus X-3 or Hercules X-1 in a angular bin of fixed radius. The medians of the energy distributions determine the median energies for cosmic ray particles from the direction of Cygnus X-3 and Hercules X-1 that would trigger the experiment and pass all selection criteria. By normalizing our energy scale to the cosmic ray flux, we make the assumption that the primary particle has the same spectral index as the detected cosmic rays. This assumption is reasonable when dealing with sources like Cygnus X-3 and Hercules X-1 in which there are no well established measurements of spectral indices. The median energy of particles from the direction of Cygnus X-3 is 114 TeV, and from Hercules X-1, it is 116 TeV. Since the difference in the energies for the two sources is negligible, we report our measurements at a common energy of 115 TeV.

5.5 Search Strategy

We carry out searches for particle emission from a particular source by comparing the number of events found within a circular angular bin around the source to the number of events estimated by

Table 5: Data samples selected by integral cuts on the number of CASA alerts. The cut values are given in the first column and the fractions of events surviving the cut (and within the angular search region) are shown in the second column. The median energies for events coming from either Cygnus X-3 or Hercules X-1 are listed in the third column.

| Alert Cut | Event Fraction | Median Energy |
|-----------|----------------|---------------|
| None | 100.00% | 115 TeV |
| ≤ 10 | 62.87% | 85 TeV |
| > 40 | 0.58% | 530 TeV |
| > 80 | 0.09% | 1175 TeV |

our background procedure. The angular bin sizes vary as a function of the number of alerted CASA stations, as itemized in Table 3. Source positions (J1992) are taken to be $(\alpha, \delta) = (308.04^\circ, 40.93^\circ)$ for Cygnus X-3, and $(\alpha, \delta) = (254.39^\circ, 35.35^\circ)$ for Hercules X-1.

Separate searches are made based on particle type and energy. By using the *all-data* sample, we are sensitive to any type of neutral particle that would create air showers. With the *muon-poor* sample, we are specifically sensitive to the emission of gamma-rays. We carry out three separate searches with various integral cuts on the number of alerted CASA stations, in addition to a search with no cuts. This procedure takes advantage of the correlation between primary energy and size (as represented by the number of alerts), and improves our sensitivity to possible emission that might be present at either low or high energies. The data samples selected by cutting on the alert number and their corresponding median energies are shown in Table 5.

6 Results

We search for evidence of neutral (gamma-ray or other) particle emission from Cygnus X-3 and Hercules X-1. Separate searches are carried out for steady and transient emission from either source. In addition, we search for periodic emission from Cygnus X-3 at the 4.8 hr X-ray periodicity and for emission from Cygnus X-3 that was coincident with the occurrence of large radio flares. No compelling evidence for emission from either source is found for all the different searches, and consequently we set upper limits on the fluxes of particles from the sources.

6.1 Steady Emission

The numbers of on-source and background events for the various searches from Cygnus X-3 are shown in Table 6. The results from similar searches carried out on Hercules X-1 are shown in Table 7. For each search, we also calculate the statistical significance of any excess or deficit in the number of events observed relative to background by the prescription of Li and Ma [88], using an oversampling factor of 10. No significant excess is observed for any search from either source. Therefore, for each search, we calculate an upper limit, N_{90} , on the number of excess events from the source at the 90% confidence level [89, 90]. Each N_{90} value is converted to a limit on the fractional excess of events from the source, f_{90} , by dividing by the estimated number of background events, which is assumed to represent the background cosmic-ray level. Since the f_{90} values are independent of the absolute flux normalization, they are useful in comparing results between different experiments.

Table 6: Steady emission search results for Cygnus X-3 using the all-data sample (top) and muon-poor sample (bottom). The number of events observed on-source and the number expected from background are given in the second the third columns, respectively. The fourth column gives the statistical significance of any excess or deficit. The 90% c.l. upper limit on the number of excess events, N_{90} , and the upper limit on the fractional excess, f_{90} , are given in the last two columns. The methods used to calculate statistical significances and upper limits are outlined in the text. The data samples at 85 TeV, 530 TeV, and 1175 TeV are subsets of the data sample at 115 TeV.

| All-Data Sample | | | | | |
|-----------------|-----------|------------|---------------|----------|-----------------------|
| Energy | On-Source | Background | Signif. | N_{90} | f_{90} |
| 85 TeV | 1119469 | 1119987 | -0.48σ | 1502.1 | 1.34×10^{-3} |
| 115 TeV | 1780594 | 1781479 | -0.66σ | 1774.9 | 9.96×10^{-4} |
| 530 TeV | 10286 | 10235 | $+0.49\sigma$ | 205.3 | 2.01×10^{-2} |
| 1175 TeV | 1583 | 1580 | $+0.08\sigma$ | 68.9 | 4.36×10^{-2} |

| Muon-Poor Sample | | | | | |
|------------------|-----------|------------|---------------|----------|-----------------------|
| Energy | On-Source | Background | Signif. | N_{90} | f_{90} |
| 85 TeV | 149676 | 149863 | -0.57σ | 548.1 | 5.90×10^{-4} |
| 115 TeV | 121409 | 121594 | -0.37σ | 485.4 | 3.28×10^{-4} |
| 530 TeV | 20 | 21.0 | -0.21σ | 8.2 | 9.47×10^{-4} |
| 1175 TeV | 1 | 0.6 | $+0.44\sigma$ | 3.5 | 2.67×10^{-3} |

Table 7: Steady emission search results for Hercules X-1 using the all-data sample (top) and muon-poor sample (bottom).

| All-Data Sample | | | | | |
|-----------------|-----------|------------|---------------|----------|-----------------------|
| Energy | On-Source | Background | Signif. | N_{90} | f_{90} |
| 85 TeV | 1058904 | 1057583 | $+1.12\sigma$ | 2738.1 | 2.59×10^{-3} |
| 115 TeV | 1681708 | 1681392 | $+0.23\sigma$ | 2387.6 | 1.42×10^{-3} |
| 530 TeV | 9579 | 9532 | $+0.46\sigma$ | 196.5 | 2.06×10^{-2} |
| 1175 TeV | 1419 | 1459 | -0.98σ | 44.0 | 3.02×10^{-2} |

| Muon-Poor Sample | | | | | |
|------------------|-----------|------------|---------------|----------|-----------------------|
| Energy | On-Source | Background | Signif. | N_{90} | f_{90} |
| 85 TeV | 139580 | 139670 | -0.24σ | 577.1 | 6.57×10^{-4} |
| 115 TeV | 113360 | 113244 | $+0.37\sigma$ | 643.4 | 4.62×10^{-4} |
| 530 TeV | 14 | 16.8 | -0.67σ | 6.3 | 7.96×10^{-4} |
| 1175 TeV | 0 | 0.5 | -0.98σ | 2.3 | 1.90×10^{-3} |

Table 8: Flux limits from searches for steady emission from Cygnus X-3 (top) and Hercules X-1 (bottom). The second and third columns give the 90% c.l. upper limit on the integral flux of any neutral or gamma-ray particles from the source, respectively. The units of flux are particles $\text{cm}^{-2} \text{sec}^{-1}$.

| Cygnus X-3 | | |
|------------|------------------------|------------------------|
| Energy | $\Phi_N (E)$ | $\Phi_\gamma (E)$ |
| 115 TeV | 2.20×10^{-14} | 6.26×10^{-15} |
| 530 TeV | 1.43×10^{-15} | 1.21×10^{-16} |
| 1175 TeV | 1.04×10^{-15} | 5.19×10^{-17} |

| Hercules X-1 | | |
|--------------|------------------------|------------------------|
| Energy | $\Phi_N (E)$ | $\Phi_\gamma (E)$ |
| 115 TeV | 3.04×10^{-14} | 8.55×10^{-15} |
| 530 TeV | 2.87×10^{-15} | 9.75×10^{-17} |
| 1175 TeV | 6.91×10^{-16} | 3.56×10^{-17} |

Figure 7 shows scans in right ascension for bands of declination centered on Cygnus X-3 for the all-data and muon-poor samples. No significant excess above background is seen in either sample for the bin containing Cygnus X-3. The background estimation agrees well with the data in the off-source region. Similar scans for Hercules X-1 are shown in Figure 8, and again the background estimation agrees well with the observed data and no excesses are seen.

6.1.1 Flux Limit Calculation

In the absence of a statistically significant excess from either Cygnus X-3 or Hercules X-1, we set upper limits on the flux of particles from each source. Separate limits are set for neutral and gamma-ray primaries. For gamma-ray primaries, the 90% c.l. upper limit, $\Phi_\gamma(E)$, on the integral flux is calculated from the measured fractional excess by normalizing to the cosmic ray flux:

$$\Phi_\gamma (E) = \frac{f_{90} \bar{\Omega}}{\epsilon R_\gamma} J(E) . \quad (3)$$

Here, $\bar{\Omega}$ is the mean solid angle used in the search, ϵ is the fraction of events that would pass cuts and fall into the search bin, $J(E)$ is the integral cosmic ray intensity above energy E , and R_γ is a factor which accounts for the relative trigger efficiency for gamma-rays as opposed to cosmic rays. The value of $\bar{\Omega}$ ranges from $5.74 \times 10^{-3} \text{sr}$ for the lowest energy data set to $1.60 \times 10^{-4} \text{sr}$ for the highest energy data set. The ϵ factor accounts for the fraction of gamma-rays that would end up in the angular search bin (0.72) and the fraction that would pass the muon-poor selection criterion (Table 4). The value of R_γ was determined by Monte Carlo simulations to be 1.6.

To determine an upper limit on the integral flux of any neutral particle from a source, $\Phi_N(E)$, we use Eq. 3, except ϵ is now 0.72 and R_γ is 1.0. In this calculation, we assume that the neutral particle would interact in the atmosphere to create air showers in a similar manner to cosmic rays.

Table 8 gives the flux limits obtained from the various searches for steady emission from the two sources. Limits are not calculated for the data samples with median energies of 85 TeV because these are *not* integral energy samples.

6.2 Transient Emission

We search for transient emission of particles from Cygnus X-3 and Hercules X-1 on daily (single transit) time scales. For each transit of the source, we compare the number of on-source events to the number of expected background events and calculate a significance based on the prescription of Li and Ma [88]. We require the live time fraction during the transit to be at least 0.20 to remove transits in which the experiment was operational for only a small fraction of the time. For each source, we make separate studies of the transit significances for the all-data and muon-poor samples, corresponding to possible emission from any neutral and gamma-ray particles, respectively.

For Cygnus X-3, the number of good transits in the all-data sample is 1500. In the muon-poor sample, it is 1291. The distributions of significances for the two samples of Cygnus X-3 transits are shown in Figure 9. Each distribution agrees well with a Gaussian distribution of mean zero and unit width. There is no evidence for any excess of events at high values of significance (either positive or negative).

For Hercules X-1, there are 1492 good transits in the all-data sample, and 1271 good transits in the muon-poor sample. The significance distributions for Hercules X-1 are shown in Figure 10, and again, no evidence for significant excesses exists.

Based on the lack of statistically significant excesses, we place limits on the daily fluxes of neutral and gamma-ray particles from Cygnus X-3 and Hercules X-1. These limits are calculated by a similar procedure as used for the steady searches. The limit values depend on the actual statistical significance of the search on a given day, and also on the epoch of data taking. As shown in Table 1, the size of the experiment has changed with time, and the sensitivity changed accordingly. In Table 9, we give typical daily flux limits for the two sources for different epochs of the experiment. Since the numbers of events detected per transit are the same for the two sources to within 5%, the limits for Cygnus X-3 and Hercules X-1 are virtually identical. Typical 90% c.l. limits on the integral flux using the full experiment are $\Phi_N(E > 115 \text{ TeV}) < 9.7 \times 10^{-13}$ neutral particles $\text{cm}^{-2} \text{ sec}^{-1}$ and $\Phi_\gamma(E > 115 \text{ TeV}) < 2.0 \times 10^{-13}$ photons $\text{cm}^{-2} \text{ sec}^{-1}$.

We have also carried out searches for transient emission on the shorter time scale of 0.5 hr. Here, we compare the number of events observed on-source to the expected background level for ten 0.5 hr time intervals on either side of the time of source culmination. The typical number of on-source events, and therefore the flux sensitivity, depends strongly on the source zenith angle. For example, for an overhead source near culmination, the experiment observes ~ 175 events per 0.5 hr, whereas at four hours from culmination the rate is ~ 15 events per 0.5 hr. Regardless of the rate, for each 0.5 hr interval, we calculate the significance in the number of on-source events relative to the background and combine all such significances into a single distribution. The resulting significance distributions are consistent with those expected from background processes for both sources in both the all-data and muon-poor samples. The typical 90% c.l. upper limits on the fluxes from either source are $\Phi_N(E > 115 \text{ TeV}) < 3.1 \times 10^{-12}$ neutral particles $\text{cm}^{-2} \text{ sec}^{-1}$ and $\Phi_\gamma(E > 115 \text{ TeV}) < 7.1 \times 10^{-13}$ photons $\text{cm}^{-2} \text{ sec}^{-1}$ for 0.5 hr periods within one hour of culmination.

6.2.1 Cygnus X-3 Radio Flares

We study showers from the direction of Cygnus X-3 during the occurrence of large radio flares at the source. We define large flares as those times when the radio output at 8.3 GHz exceeded 2 Jy, a level which is two orders of magnitude above the typical quiescent level. During the period of CASA-MIA operations, there were six large flares, as listed in Table 10 [12, 13].

Table 9: Typical daily upper flux limits (90% c.l.) for emission of neutral and gamma-ray particles from Cygnus X-3 and Hercules X-1. The flux limits are calculated for two different epochs assuming the same number of on-source events as off-source. The third column gives the typical number of events observed on-source during the different epochs. Epoch I corresponds to March 1990 to October 1990. Epoch II corresponds to January 1992 to August 1993. Flux limits for the remaining periods of time of operation are close to those for Epoch II. Units of flux are particles $\text{cm}^{-2} \text{sec}^{-1}$.

| Epoch I | | | | |
|----------|---------------|--------|----------|-----------------------|
| Energy | Particle | Events | f_{90} | $\Phi_{daily}(E)$ |
| 115 TeV | Any | 575 | 0.071 | 1.6×10^{-12} |
| 530 TeV | Any | 3.2 | 1.34 | 1.9×10^{-13} |
| 1175 TeV | Any | 0.56 | 4.11 | 9.6×10^{-14} |
| 115 TeV | γ -ray | 45 | 0.026 | 3.6×10^{-13} |

| Epoch II | | | | |
|----------|---------------|--------|----------|-----------------------|
| Energy | Particle | Events | f_{90} | $\Phi_{daily}(E)$ |
| 115 TeV | Any | 1450 | 0.044 | 9.7×10^{-13} |
| 530 TeV | Any | 8.1 | 0.76 | 1.1×10^{-13} |
| 1175 TeV | Any | 1.3 | 2.56 | 5.9×10^{-14} |
| 115 TeV | γ -ray | 96 | 0.015 | 2.0×10^{-13} |

Table 10: Large radio flares of Cygnus X-3 from 1990 to 1995, coincident with the operational time of CASA-MIA. The flare number is an arbitrary index used for this work. The peak radio flux values (8.3 GHz) come from [12, 13]. The March 1994 flare was actually a prolonged event that extended for the ten days following March 1, 1994.

| Flare | Date | Peak Flux (Jy) |
|-------|---------------|----------------|
| 1 | Aug. 15, 1990 | 7.5 |
| 2 | Oct. 05, 1990 | 10.2 |
| 3 | Jan. 21, 1991 | 14.8 |
| 4 | Sep. 04, 1992 | 4.1 |
| 5 | Feb. 20, 1994 | 4.9 |
| 6 | Mar. 09, 1994 | 5.2 |

Table 11: CASA-MIA search results for emission from Cygnus X-3 near the time of large radio flares. The flare numbers are defined in Table 10. The $-$ and $+$ designations refer to the days preceding and following the flare day, respectively. The significances (columns 4 and 8) are standard deviation values calculated using the prescription of Li and Ma [88]. The last two columns give the 90% c.l. upper limits on the integral flux above 115 TeV of any neutral particle and gamma-rays, respectively, in units of 10^{-12} particles $\text{cm}^{-2} \text{sec}^{-1}$. Entries having only a dash indicate the absence of any usable data.

| Flare | All-Data Sample | | | | Muon-Poor Sample | | | | Flux Limits | |
|-------|-----------------|--------|---------|--------------|------------------|-------|---------|--------------|-------------|------------------|
| | On | Back | Signif. | $f_{90}(\%)$ | On | Back | Signif. | $f_{90}(\%)$ | $\Phi_N(E)$ | $\Phi_\gamma(E)$ |
| $-$ | 226 | 241.2 | -0.94 | 7.8 | $-$ | $-$ | $-$ | $-$ | 1.7 | $-$ |
| 1 | 249 | 249.5 | -0.03 | 10.8 | $-$ | $-$ | $-$ | $-$ | 2.4 | $-$ |
| $+$ | 252 | 248.1 | $+0.25$ | 12.1 | 22 | 19.4 | $+0.58$ | 5.2 | 2.7 | 0.73 |
| $-$ | 850 | 863.1 | -0.43 | 4.9 | 121 | 113.4 | $+0.67$ | 3.4 | 1.1 | 0.48 |
| 2 | 884 | 849.1 | $+1.13$ | 9.0 | 94 | 111.7 | -1.65 | 1.5 | 2.0 | 0.21 |
| $+$ | 872 | 901.4 | -0.94 | 3.9 | 103 | 124.5 | -1.90 | 1.4 | 0.9 | 0.20 |
| $-$ | 1279 | 1260.1 | $+0.51$ | 5.8 | 227 | 230.7 | -0.23 | 2.3 | 1.3 | 0.32 |
| 3 | 1297 | 1267.3 | $+0.80$ | 6.4 | 255 | 235.5 | $+1.19$ | 4.0 | 1.4 | 0.56 |
| $+$ | 1265 | 1235.2 | $+0.81$ | 6.6 | 216 | 227.2 | -0.71 | 1.9 | 1.5 | 0.27 |
| $-$ | 884 | 992.8 | $+0.04$ | 5.8 | 59 | 50.2 | $+1.15$ | 2.8 | 1.3 | 0.39 |
| 4 | 711 | 756.9 | -1.61 | 3.4 | 45 | 53.4 | -1.13 | 1.4 | 0.8 | 0.20 |
| $+$ | 735 | 773.9 | -1.35 | 3.7 | 30 | 43.4 | -2.07 | 0.9 | 0.8 | 0.13 |
| $-$ | 1708 | 1734.0 | -0.60 | 3.2 | 119 | 126.9 | -0.68 | 1.1 | 0.7 | 0.15 |
| 5 | 1692 | 1596.2 | $+2.26$ | 9.4 | 119 | 124.4 | -0.47 | 1.2 | 2.1 | 0.17 |
| $+$ | 1485 | 1447.1 | $+0.95$ | 6.4 | 127 | 119.1 | $+0.68$ | 2.1 | 1.4 | 0.29 |
| $-$ | 1382 | 1375.2 | $+0.18$ | 4.9 | 92 | 102.6 | -1.02 | 1.1 | 1.1 | 0.15 |
| 6 | 1212 | 1225.3 | -0.36 | 4.2 | 90 | 95.1 | -0.50 | 1.4 | 0.9 | 0.20 |
| $+$ | 1390 | 1391.7 | -0.06 | 4.4 | 108 | 99.1 | $+0.84$ | 2.1 | 1.0 | 0.29 |

We examine the daily significances for Cygnus X-3 on the day of each large flare, as well as on the day preceding and following each flare. Table 11 lists the numbers of observed events, the expected background, and the Li-Ma significances for the examined days. There is no compelling evidence for any statistical excess in the observed number of events from Cygnus X-3 for either the all-data or muon-poor samples. On one day (Feb. 20, 1994) the Li-Ma significance is 2.26σ for the all-data sample. The probability that we would get a day with this level of significance or greater is 28.2% after accounting for the fifteen days in which we searched. In addition, on this same day, there is no evidence for any excess in the muon-poor data, while we would expect the statistical significance to increase by a factor of 3.3 if it were due to a gamma-ray signal. Table 11 also lists the derived fractional excess values, f_{90} , as well as the upper limits to the integral flux of neutral or gamma-ray particles from Cygnus X-3 during the flares.

6.3 Periodic Emission

Several previous observations of Cygnus X-3 claimed evidence for steady emission correlated with the 4.8 hr X-ray periodicity of the source. For this reason, we carry out a search for such emission

Table 12: CASA-MIA search results for 4.8 hr periodic emission from Cygnus X-3. Flux limits are given for selected phase intervals in which earlier experiments had reported detections. Columns 3 and 4 give the 90% c.l. upper limits to the integral flux of neutral and gamma-ray particles, respectively, in units of particles $\text{cm}^{-2} \text{sec}^{-1}$. A blank entry corresponds to a data set having insufficient data with which to calculate a limit.

| Phase Interval | Energy | $\Phi_N(E)$ | $\Phi_\gamma(E)$ |
|----------------|----------|-----------------------|-----------------------|
| 0.2 – 0.3 | 115 TeV | 8.9×10^{-14} | 2.3×10^{-14} |
| | 530 TeV | 4.5×10^{-15} | 6.9×10^{-16} |
| | 1175 TeV | 3.5×10^{-15} | – |
| 0.6 – 0.7 | 115 TeV | 1.4×10^{-13} | 3.5×10^{-14} |
| | 530 TeV | 3.8×10^{-15} | 3.4×10^{-16} |
| | 1175 TeV | 6.5×10^{-15} | – |

using the entire CASA-MIA data set. The event arrival times (UT) are corrected to the barycenter of the solar system using the JPL DE200 planetary ephemeris [91]. The corrected times are folded with the 4.8 hr X-ray ephemeris of van der Klis and Bonnet-Bidaud [8]. A slight correction is made for newer X-ray data from the ASCA satellite, as reported by Kitamoto *et al.* [9]. Each event is then assigned a phase value in the interval (0,1) representing the fraction of a period that the event is from the X-ray minimum. The phase values are accumulated in twenty bins of 0.05 phase units each for both the on-source and generated background events.

Figure 11 shows the 4.8 hr periodicity distribution of events from the direction of Cygnus X-3 for the all-data and muon-poor samples. Also shown is the phase distribution expected from the background events. No compelling excesses are seen at any particular phase interval for either sample. We carry out similar periodicity analyses using data at higher energies selected by the number of alerted CASA stations. These searches also do not indicate any significant excesses at any phase interval. In Table 12, we list flux limits for the various searches at the phase intervals (0.2,0.3) and (0.6,0.7). These intervals were ones in which numerous earlier experiments had reported detections.

7 Comparison with Other Results

As described earlier, the many detections of Cygnus X-3 and Hercules X-1 by experiments operating between 1975 and 1990 varied greatly in their characteristics. Some results were steady and some were episodic; some exhibited apparent periodicity and others did not. We thus choose to compare the results of this work to a generalized picture of the earlier results and to more recent work.

7.1 Cygnus X-3

In Figure 12, we plot the flux limits reported here on steady emission from Cygnus X-3. We also show published results from other experiments using data taken at times which overlap our observation period. The other results come from the Tibet air shower array in Yangbajing, China [92], the CYGNUS array in New Mexico, USA [93], the EAS-TOP array at Gran Sasso, Italy [94], and the HEGRA experiment on the Canary Island La Palma [95]. We do not show earlier results

from data taken by a portion of our experiment in 1989 [46] or the results of our all-sky survey for northern hemisphere point sources using data taken in 1990-1991 [83]. In Figure 13, we show a similar comparison of the limits on the fractional excess of events from Cygnus X-3 relative to the cosmic ray background.

The data from the recent experiments are consistent; no steady emission of ultra-high energy particles (gamma-ray or otherwise) has been detected from Cygnus X-3 at levels which are considerably lower than earlier reports. At TeV energies, the results from the Whipple Telescope [96] are also considerably lower than the earlier reports. The limits presented here are a factor of 130 lower at 115 TeV, and a factor of 900 at 1175 TeV, than the spectrum plotted in Figure 1. Our results are also inconsistent with emission reported by a smaller experiment using data taken during a time that overlapped our observations [47].

The limits presented here on transient emission from Cygnus X-3 are lower than, but in agreement with, those reported by other air shower experiments. There have been no compelling reports of transient emission of gamma-rays from Cygnus X-3 over the period 1990-1995, including during large radio flares from the source. There was an observation of underground muons from the direction of Cygnus X-3 during the January 1991 radio flare [97]. The reported flux for this observation was 7.5×10^{-10} muons $\text{cm}^{-2} \text{sec}^{-1}$, for muon energies above 0.7 TeV. If the muons were produced in air showers by the interaction of a hypothetical neutral particle from Cygnus X-3, we would expect a typical neutral particle energy of ~ 10 TeV [98]. Assuming that the particle spectrum continues to energies detectable by CASA-MIA (and conservatively using a soft spectrum comparable to the cosmic rays), one derives an expected flux of $\sim 10^{-11}$ particles $\text{cm}^{-2} \text{sec}^{-1}$ for energies above 115 TeV. This flux is a factor of 5 to 10 above the flux limits set by CASA-MIA on the emission of any neutral particle during the January 1991 flare (Table 11).

We have also shown that there is no evidence for 4.8 periodic emission from Cygnus X-3. This result is consistent with reports by other experiments over the same period of time. The limits on pulsed gamma-ray emission presented here for the phase intervals of 0.2-0.3 and 0.6-0.7 (Table 12) are lower at 115 TeV, and considerably lower at 530 TeV, than the fluxes predicted by a recent theoretical paper [99].

7.2 Hercules X-1

The limits on steady emission of gamma-rays from Hercules X-1 presented here are in agreement with those from other experiments, as shown in Figure 14. Gamma-ray emission from Hercules X-1 was typically seen by earlier experiments as transient emission over short time scales (e.g. the 1986 outbursts). We have no evidence for such emission over the entire period 1990-1995. In Figure 15, we compare the daily event totals observed by CASA-MIA from the direction of Hercules X-1 to the total expected assuming the flux of an earlier reported outburst [60]. Clearly, no evidence for emission at even much weaker levels than this outburst is seen during this time. The flux reported in Ref. [60] was $\sim 2 \times 10^{-11}$ particles $\text{cm}^{-2} \text{sec}^{-1}$ for minimum energies of 100 TeV. This flux is about a factor of 45 larger than the typical limits placed by CASA-MIA during the early part of operations and about a factor of 80 larger than the typical daily gamma-ray limits placed by the full CASA-MIA experiment (Table 9). Since we have no evidence for transient emission from Hercules X-1, we choose not to carry out a periodicity analysis based on the X-ray pulsar period of 1.24 sec.

8 Conclusions

We have carried out a high statistics search for ultra-high energy neutral and gamma-ray particle emission from Cygnus X-3 and Hercules X-1 between 1990 and 1995. We have no evidence for steady or transient emission from either source, and for Cygnus X-3, we have no evidence for 4.8 hr periodic emission or emission correlated with large radio flares. These results are in agreement with those from other experiments operating during the same period of time, but are in stark contrast to earlier (1975-1990) reports.

The apparent disappearance of Cygnus X-3 and Hercules X-1 from the ultra-high energy gamma-ray sky can be interpreted in two ways. An optimistic view [3] is that the earlier results indicated the presence of ultra-high energy gamma-rays (or particles) from Cygnus X-3 and Hercules X-1, and that the sources, which are episodic on long times scales, are now dormant. A more pessimistic view is that the earlier reported detections were largely, if not entirely, statistical fluctuations, and that no compelling evidence exists for ultra-high energy gamma-rays from any astrophysical source. We point out that an earlier all-sky survey using a portion of our data sample indicates that the northern hemisphere does not contain any steady point sources of gamma-rays with fluxes comparable to those reported from X-ray binaries in the 1980's [83]. We have presented an update on this analysis at a conference [100] which are consistent with the absence of bright 100 TeV gamma-ray point sources. We are in the process of completing a final all-sky survey on the five year CASA-MIA data sample.

The pessimistic interpretation of the ultra-high energy point source question, if correct, highlights the difficulties in detecting gamma-rays from sources at other (high) energies and in detecting neutrinos as well. In addition, without compelling evidence for high energy particle acceleration at point sources, the difficulties in explaining the origins of cosmic rays above 10^{14} eV remain.

Acknowledgements

We acknowledge the assistance of the command and staff of Dugway Proving Ground, and the University of Utah Fly's Eye group. Special thanks go to M. Cassidy. We also wish to thank P.Burke, S. Golwala, M. Galli, J. He, H. Kim, L. Nelson, M. Oonk, M. Pritchard, P. Rauske, K. Riley, and Z. Wells for assistance with data processing. This work is supported by the U.S. National Science Foundation and the U.S. Department of Energy. JWC and RAO wish to acknowledge the support of the W.W. Grainger Foundation. RAO acknowledges additional support from the Alfred P. Sloan Foundation.

* Present Address: Department of Physics, Massachusetts Institute of Technology, Cambridge, MA 02139, USA.

† Present Address: Department of Physics and Astronomy, Iowa State University, Ames, IA 50011, USA.

References

- [1] For a recent review of ground-based gamma-ray astronomy, see R.C. Lamb, R.A. Ong, C.E. Covault, and D.A. Smith, *Proc. of the 1994 Snowmass Summer Study, Particle and Nuclear Astrophysics and Cosmology in the Next Millennium*, ed. by E.W. Kolb and R.D. Peccei (World Scientific, Singapore, 1995) 295.

- [2] For general reviews see: T.C. Weekes, Phys. Rep. **160**, 1 (1988); D.E. Nagle, T.K. Gaisser, and R.J. Protheroe, Annu. Rev. Nucl. Part. Sci. **38**, 609 (1988); T.C. Weekes, Space Sci. Rev. **59**, 315 (1992); J.W. Cronin, K.G. Gibbs, and T.C. Weekes, Annu. Rev. Nucl. Part. Sci. **43**, 883 (1993).
- [3] R.J. Protheroe, Astrophys. J. Suppl. **90**, 883 (1994).
- [4] J.M. Bonnet-Bidaud and G. Chardin, Phys. Rep. **170**, 325 (1988).
- [5] R. Giacconi, P. Gorenstein, H. Gursky, and J.R. Walters, Astrophys. J. **148**, L119 (1967).
- [6] D.R. Parsignault, E. Schreier, J. Grindlay, and H. Gursky, Astrophys. J. **209**, L73 (1976).
- [7] M. van der Klis and J.M. Bonnet-Bidaud, Astron. Astrophys. **95**, L5 (1981).
- [8] M. van der Klis and J.M. Bonnet-Bidaud, Astron. Astrophys. **214**, 203 (1989).
- [9] S. Kitamoto *et al.*, Publ. Astron. Soc. Japan **47**, 233 (1995).
- [10] P.C. Gregory *et al.*, Nature **239**, 440 (1972).
- [11] K.J. Johnston *et al.*, Astrophys. J. **309**, 707 (1986).
- [12] E.B. Waltman *et al.*, Astronom. J. **108**, 179 (1994).
- [13] E.B. Waltman *et al.*, Astronom. J. **110**, 290 (1995).
- [14] Robert Lauqué, James Lequeux, and Nguyen-Quang-Rieu, Nature Physical Science **239**, 119 (1972).
- [15] R.C. Lamb *et al.*, Astrophys. J. **212**, L63 (1977).
- [16] K. Bennett *et al.*, Astron. Astrophys. **59**, 273 (1977).
- [17] W. Hermsen *et al.*, Astron. Astrophys. **175**, 141 (1987).
- [18] C.E. Fichtel *et al.*, Astrophys. J. **319**, 362 (1987).
- [19] Ti-Pei Li and Mei Wu, Astrophys. J. **346**, 391 (1989).
- [20] P.F. Michelson *et al.*, Astrophys. J. **401**, 724 (1992).
- [21] Yu.I. Neshpor *et al.*, Astrophys. Space Sci. **61**, 349 (1979).
- [22] S. Danaher, D.J. Fegan, N.A. Porter, and T.C. Weekes, Nature **289**, 568 (1981).
- [23] R.C. Lamb, C.P. Godfrey, W.A. Wheaton, and T. Tumer, Nature **296**, 543 (1982).
- [24] J.C. Douthwaite *et al.*, Astron. Astrophys. **126**, 1 (1983).
- [25] M.F. Cawley *et al.*, Astrophys. J. **296**, 185 (1985).
- [26] P.M. Chadwick *et al.*, Nature **318**, 642 (1985).
- [27] C.L. Bhat, M.L. Sapru, and H. Razdan, Astrophys. J. **306**, 587 (1986).
- [28] K.T.S. Brazier *et al.*, Astrophys. J. **350**, 745 (1990).

- [29] A.A. Gregory *et al.*, *Astron. Astrophys.* **237**, L5 (1990).
- [30] M. Samorski and W. Stamm, *Astrophys. J.* **268**, L17 (1983).
- [31] J. Lloyd-Evans *et al.*, *Nature* **305**, 784 (1983).
- [32] T. Kifune *et al.*, *Astrophys. J.* **301**, 230 (1986).
- [33] V.V. Alexeenko *et al.*, *Il Nuovo Cimento* **10C**, 151 (1987).
- [34] R.M. Baltrusaitis *et al.*, *Astrophys. J.* **323**, 685 (1987).
- [35] S.C. Tonwar, N.V. Gopalakrishnan, M.R. Rajeev, and B.V. Sreekantan, *Astrophys. J.* **330**, L107 (1988).
- [36] C. Morello, L. Periale, P. Vallania, and G. Navarra, *Il Nuovo Cimento* **13C**, 453 (1990).
- [37] G.L. Cassiday *et al.*, *Phys. Rev. Lett.* **62**, 383 (1989).
- [38] M. Teshima *et al.*, *Phys. Rev. Lett.* **64**, 1628 (1990).
- [39] M.A. Lawrence, D.C. Prosser, and A.A. Watson, *Phys. Rev. Lett.* **63**, 1121 (1989).
- [40] M.F. Cawley and T.C. Weekes, *Astron. Astrophys.* **133**, 80 (1984).
- [41] B.L. Dingus *et al.*, *Phys. Rev. Lett.* **60**, 1785 (1988).
- [42] D.J. Fegan *et al.*, *Astron. Astrophys.* **211**, L1 (1989).
- [43] G.L. Cassiday *et al.*, *Phys. Rev. Lett.* **63**, 2329 (1989).
- [44] D.E. Alexandreas *et al.*, *Phys. Rev. Lett.* **64**, 2973 (1990).
- [45] D. Ciampa *et al.*, *Phys. Rev.* **D42**, 281 (1990).
- [46] J.W. Cronin *et al.*, *Phys. Rev.* **D45**, 4385 (1992).
- [47] Y. Muraki *et al.*, *Astrophys. J.* **373**, 657 (1991).
- [48] C.C.G. Bowden *et al.*, *J. Phys. G* **18**, 413 (1992).
- [49] S.C. Tonwar *et al.*, *Astrophys. J.* **390**, 273 (1992).
- [50] H. Tananbaum *et al.*, *Astrophys. J.* **174**, L143 (1972).
- [51] Christine A. Jones, William Forman, and William Liller, *Astrophys. J.* **182**, L109 (1973).
- [52] William Forman, Christine A. Jones, and William Liller, *Astrophys. J.* **177**, L103 (1972).
- [53] J.E. Deeter, P.E. Boynton, and S.H. Pravdo, *Astrophys. J.* **247**, 1003 (1981).
- [54] J.C. Douthwaite *et al.*, *Nature* **309**, 691 (1984).
- [55] R.M. Baltrusaitis *et al.*, *Astrophys. J.* **293**, L69, (1985).
- [56] P.W. Gorham *et al.*, *Astrophys. J.* **308**, L11 (1986).
- [57] P.W. Gorham *et al.*, *Astrophys. J.* **309**, 114 (1986).

- [58] L.K. Resvanis *et al.*, *Astrophys. J.* **328**, L9 (1988).
- [59] R.C. Lamb *et al.*, *Astrophys. J.* **328**, L13 (1988).
- [60] B.L. Dingus *et al.*, *Phys. Rev. Lett.* **61**, 1906 (1988).
- [61] P.R. Vishwanath, P.N. Bhat, P.V. Ramanamurthy, and B.V. Sreekantan, *Astrophys. J.* **342**, 489 (1989).
- [62] S.K. Gupta *et al.*, *Astrophys. J.* **354**, L13 (1990).
- [63] P.T. Reynolds *et al.*, *Astrophys. J.* **382**, 640 (1991).
- [64] D.E. Alexandreas *et al.*, *Astrophys. J.* **383**, L53 (1991).
- [65] K.S. Cheng, C. Ho, and M. Ruderman, *Astrophys. J.* **300**, 522 (1986).
- [66] G. Chanmugam and K. Brecher, *Nature* **313**, 767 (1985).
- [67] W.Thomas Vestrand and David Eichler, *Astrophys. J.* **261**, 251 (1982).
- [68] David Eichler and W.Thomas Vestrand, *Nature* **307**, 613 (1984).
- [69] Demosthenes Kazanas and Donald C. Ellison, *Nature* **319**, 380 (1986).
- [70] J. Wdowczyk and A.W. Wolfendale, *Nature* **305**, 609 (1983).
- [71] A.M. Hillas, *Nature* **312**, 50 (1984).
- [72] David Eichler and W.Thomas Vestrand, *Nature* **318**, 345 (1985).
- [73] Peter W. Gorham and John G. Learned, *Nature* **323**, 422 (1986).
- [74] K.S. Cheng and Malvin Ruderman, *Astrophys. J.* **337**, L77 (1989).
- [75] P. Slane and W.F. Fry, *Astrophys. J.* **342**, 1129 (1989).
- [76] A. Borione *et al.*, *Nucl. Inst. Meth.* **A346**, 329 (1994).
- [77] A. Borione *et al.*, *Phys. Rev.* **D49**, 1171 (1994).
- [78] M. Derrick *et al.*, *Phys. Lett.* **B293**, 465 (1992). T. Ahmed *et al.*, *Phys. Lett.* **B299**, 469 (1993).
- [79] E. Chatelet *et al.*, *J. Phys. G.* **16**, 317 (1990).
- [80] T.K. Gaisser *et al.*, *Phys. Rev.* **D43**, 314 (1991).
- [81] D.E. Alexandreas *et al.*, *Nucl. Inst. Meth.* **A328**, 570 (1993).
- [82] M. Nagano *et al.*, *J. Phys. G.* **18**, 423 (1992).
- [83] T.A. McKay *et al.*, *Astrophys. J.* **417**, 742 (1993).
- [84] A. Borione *et al.*, "A Search for Ultrahigh Energy Gamma-Ray Emission from the Crab Nebula and Pulsar," EFI 96-26 (August 1996), submitted to *The Astrophysical Journal*.
- [85] T.K. Gaisser *et al.*, *Phys. Rev. Lett.* **62**, 1425 (1989).

- [86] K. Asakimori *et al.*, Proc. 23rd Int. Cosmic Ray Conf. (Calgary), ed. D.A. Leahy, R.B. Hicks, and D. Venkatesan (World Scientific Publishing, Singapore), **2**, 21 (1994).
- [87] S.P. Swordy, Proc. 23rd Int. Cosmic Ray Conf. (Calgary), ed. D.A. Leahy, R.B. Hicks, and D. Venkatesan (World Scientific Publishing, Singapore), Rapporteur Volume, 243 (1994).
- [88] T. Li and Y. Ma, *Astrophys. J.* **272**, 317 (1983).
- [89] O. Helene, *Nucl. Inst. Meth.* **212**, 319 (1983).
- [90] Review of Particle Properties, *Phys. Rev.* **D50**, 1280 (1994).
- [91] E.M. Standish, *Astron. Astrophys.* **233**, 252 (1990).
- [92] M. Amenomori *et al.*, *Phys. Rev. Lett.* **69**, 2468 (1992).
- [93] D.E. Alexandreas *et al.*, *Astrophys. J.* **405**, 353 (1993); updated in D.E. Alexandreas *et al.*, Proc. XXIII Int. Cosmic Ray Conf. (Calgary), ed. D.A. Leahy, R.B. Hicks, and D. Venkatesan (World Scientific Publishing, Singapore), **1**, 353 (1994).
- [94] M. Aglietta *et al.*, *Astropart. Phys.* **3**, 1 (1995).
- [95] A. Karle *et al.* *Astropart. Phys.* **4**, 1 (1996).
- [96] K.S. O’Flaherty *et al.*, *Astrophys. J.* **396**, 674 (1992).
- [97] M.A. Thomson *et al.* *Phys. Lett.* **B269**, 220 (1991).
- [98] Thomas K. Gaisser, *Cosmic Rays and Particle Physics*, Cambridge University Press (1990).
- [99] Abhas Mitra, *Astrophys. J.* **425**, 782 (1994).
- [100] A. Borione *et al.*, Proc. 23rd Int. Cosmic Ray Conf. (Calgary), ed. D.A. Leahy, R.B. Hicks, and D. Venkatesan (World Scientific Publishing, Singapore), **1**, 357 (1994).

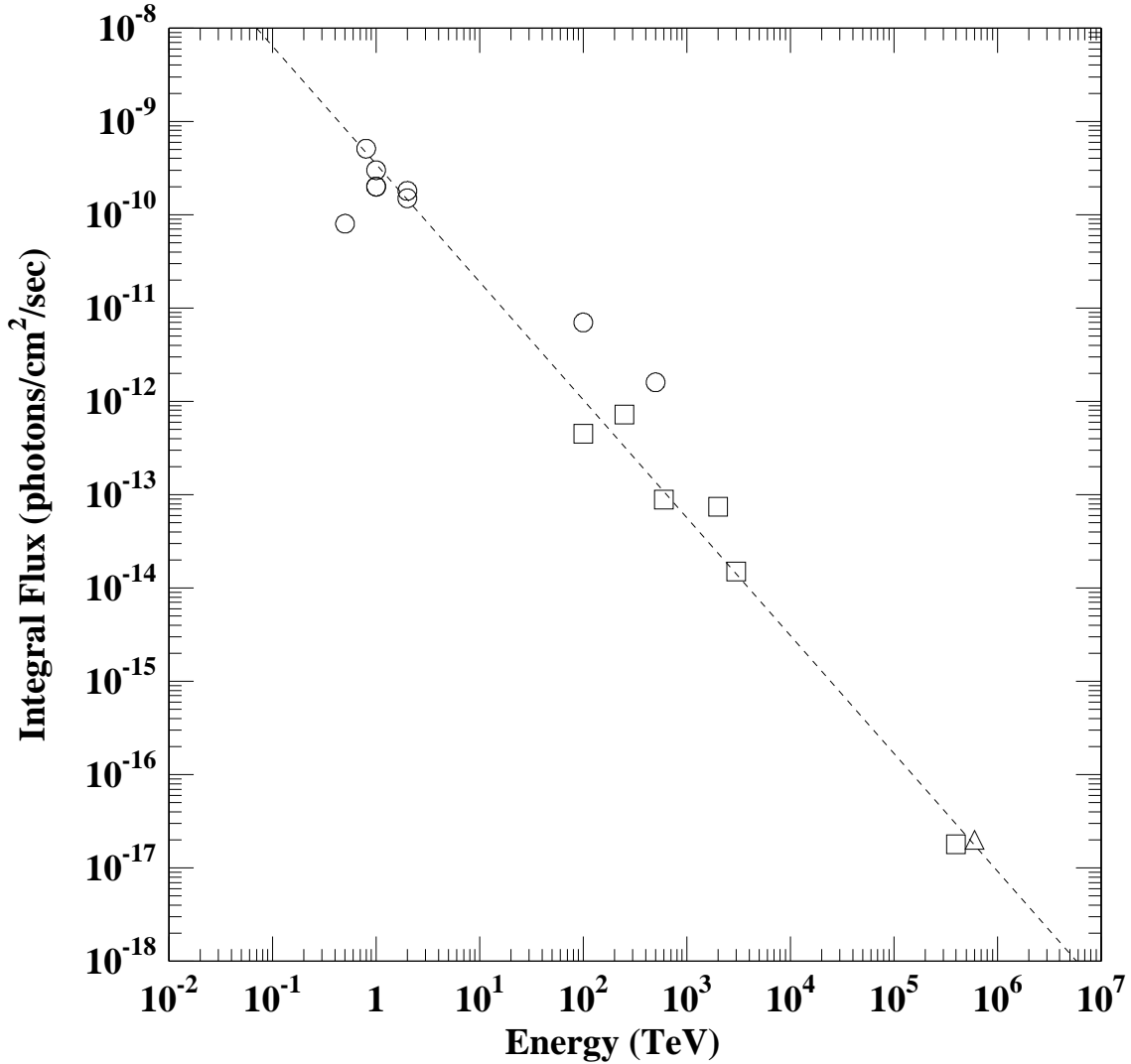


Figure 1: Published results from ground-based experiments indicating evidence for gamma-ray emission from Cygnus X-3 during the period 1975-1990. The circles indicate results from atmospheric Cherenkov telescopes, the squares show data taken by air shower arrays, and the triangle indicates the result from the Fly's Eye experiment. The dashed curve is an approximate power law fit to the data with a slope of -1.1 . Not shown in this figure are several upper limits to the flux of gamma-rays from Cygnus X-3 during this same epoch. The two points at extremely high energy (5×10^5 TeV) have been slightly displaced from each other for clarity.

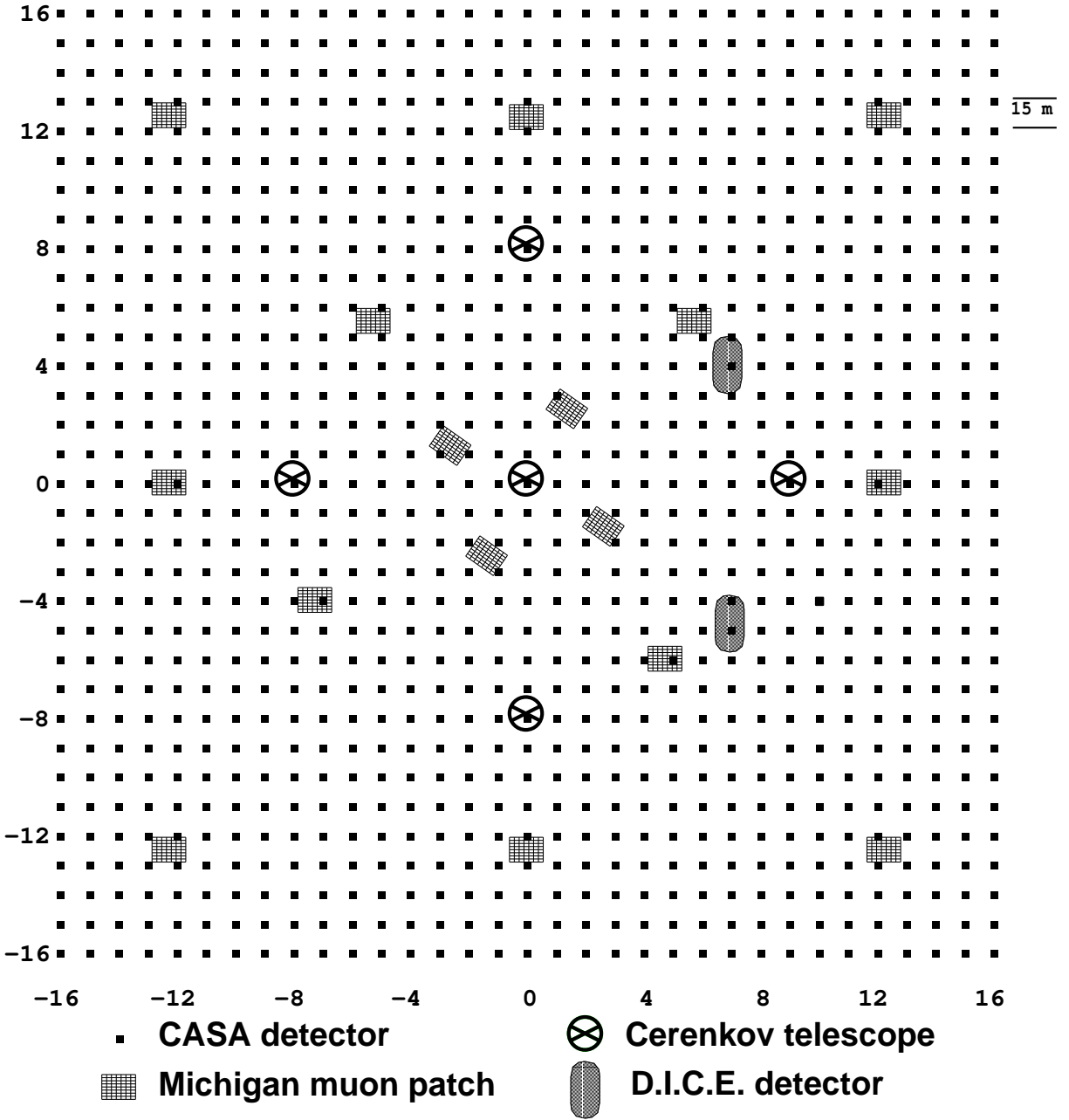


Figure 2: Plan view of the CASA-MIA experiment (Dugway, Utah, USA). Small squares indicate the 1089 scintillation detectors of the CASA surface array. Sixteen large rectangles indicate the patches of scintillation counters of the MIA underground array (64 counters/patch). Five crossed circles indicate tracking Cherenkov telescopes. The D.I.C.E. detectors are not used in this analysis.

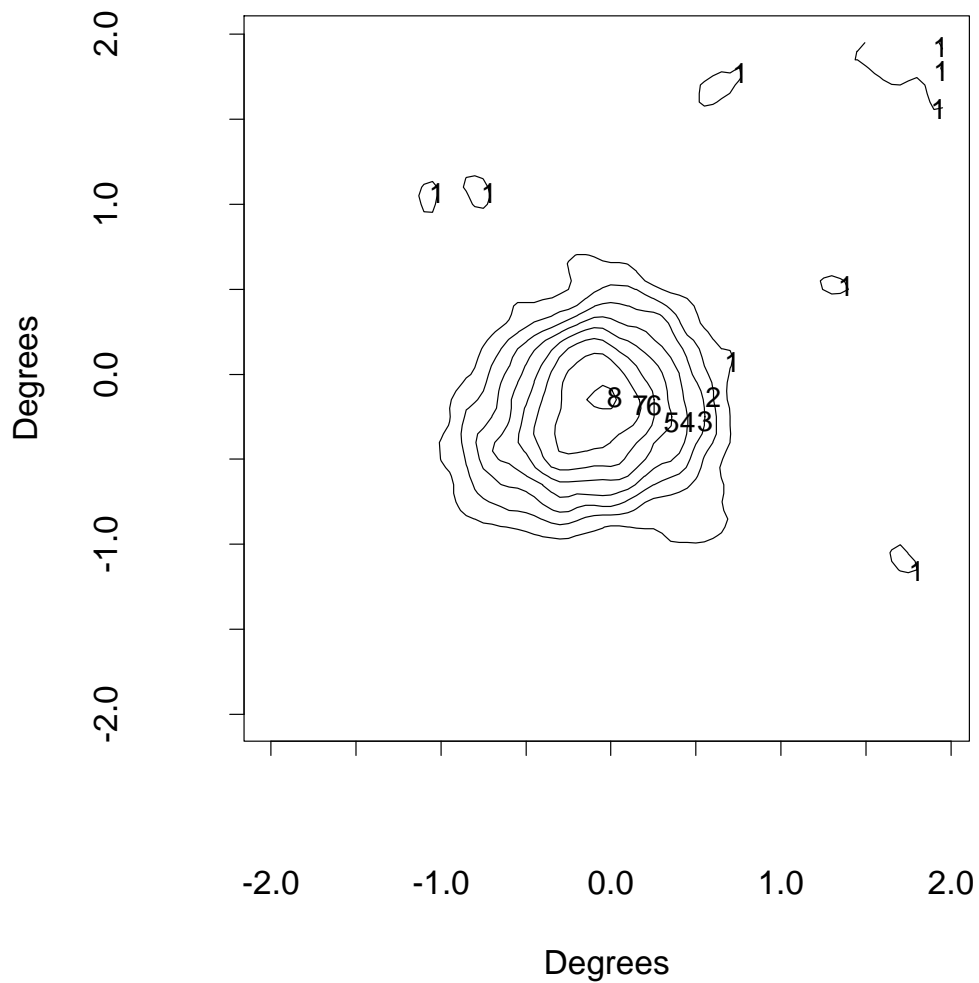


Figure 3: Shadow of the Moon as detected by CASA-MIA. The contour plot shows the deficit in the number of detected cosmic ray events as a function of the angle from the Moon center. The axes are defined by the equatorial coordinates of the Moon, with right ascension along the horizontal axis and declination along the vertical axis. The contours correspond to successive one standard deviation steps. A Gaussian smoothing factor of 0.5° has been applied to the data.

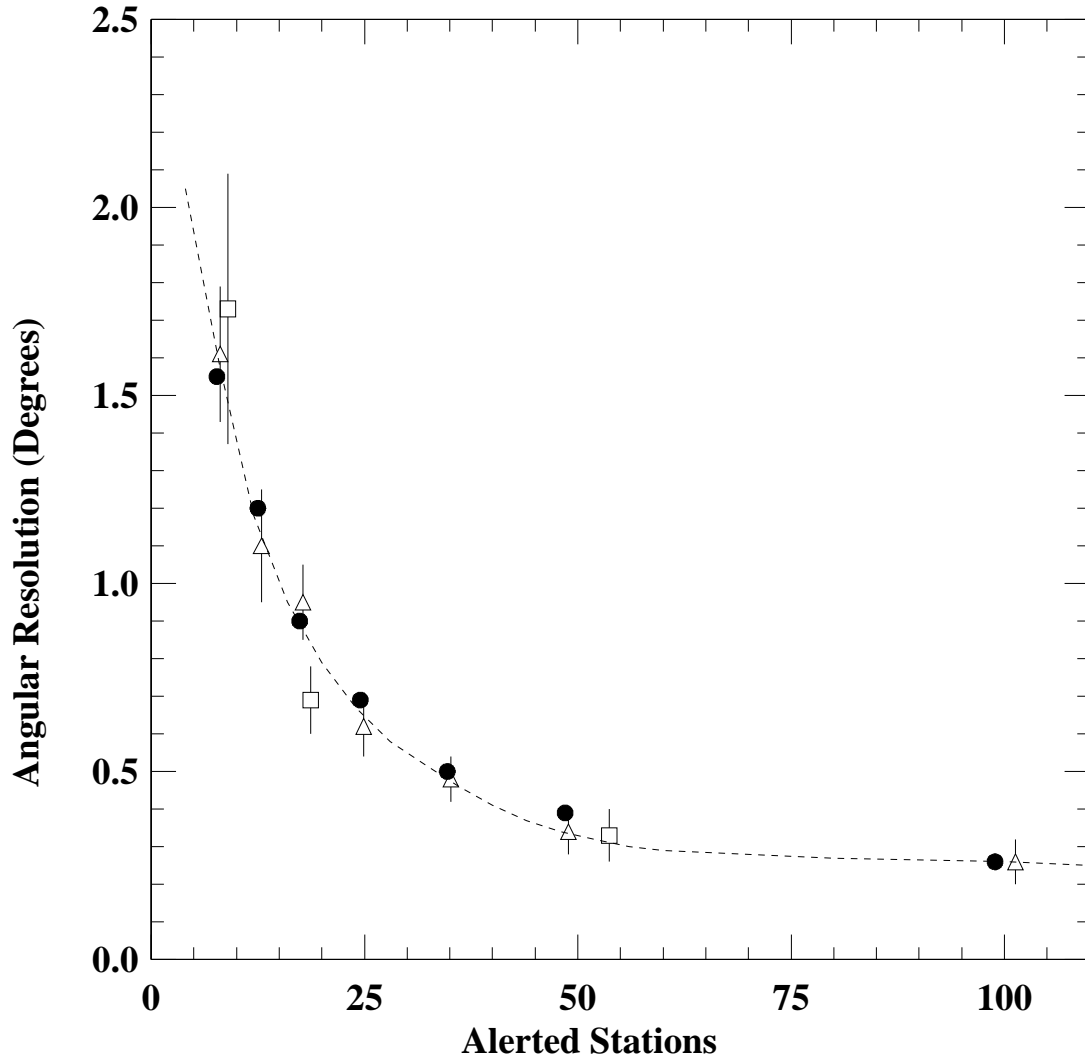


Figure 4: Angular resolution of CASA-MIA as a function of the number of alerted CASA stations. The resolution has been estimated by three different techniques: split-array method (solid points), Cherenkov telescope array coincident events (open triangles), and Moon shadow (open squares). The dashed curve indicates a simple parametric fit to the data.

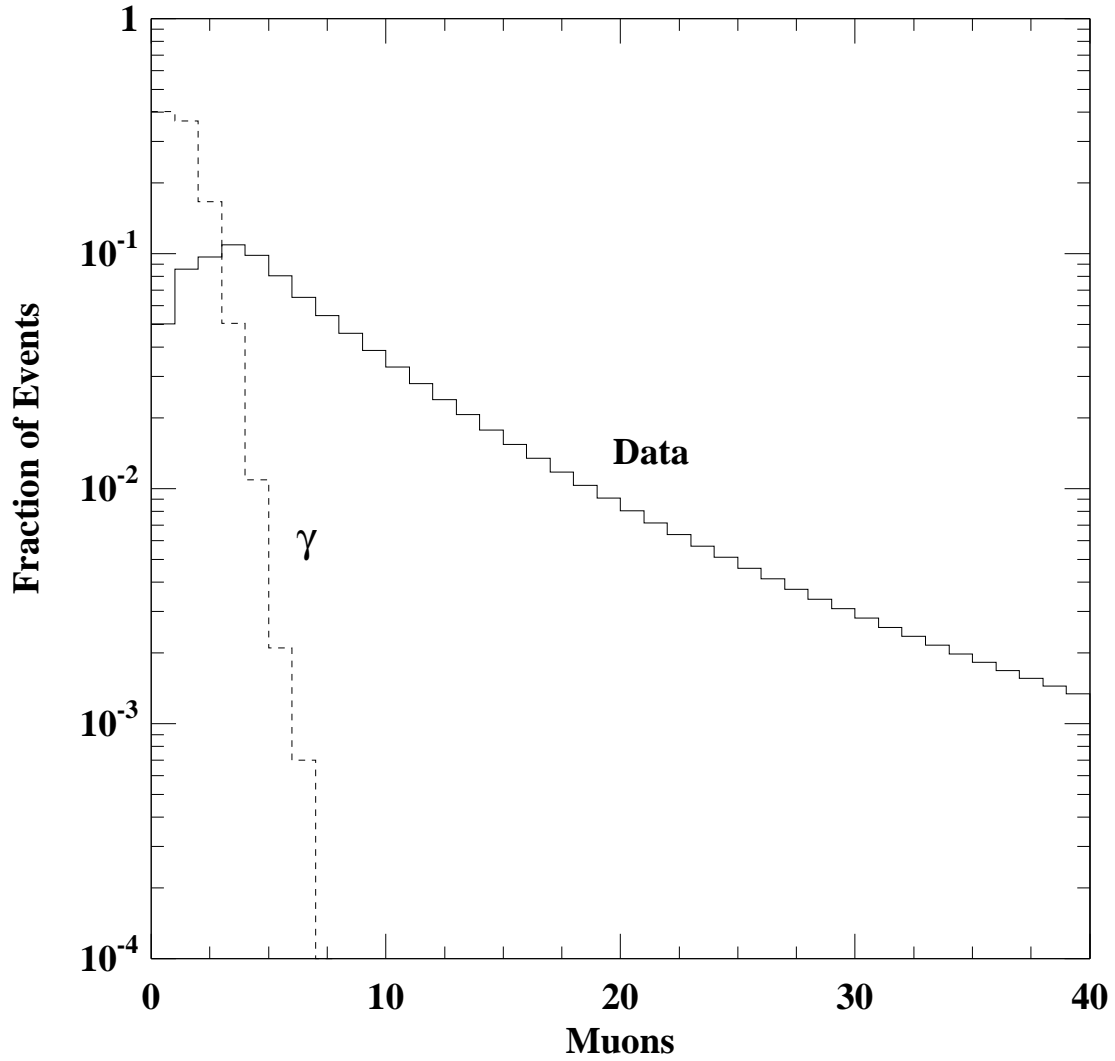


Figure 5: Histograms of the number of muons per event detected by CASA-MIA for cosmic ray data events (solid) and simulated gamma-ray events (dashed). The gamma-ray simulation uses an input energy spectrum with the same power law spectral index as the cosmic ray data.

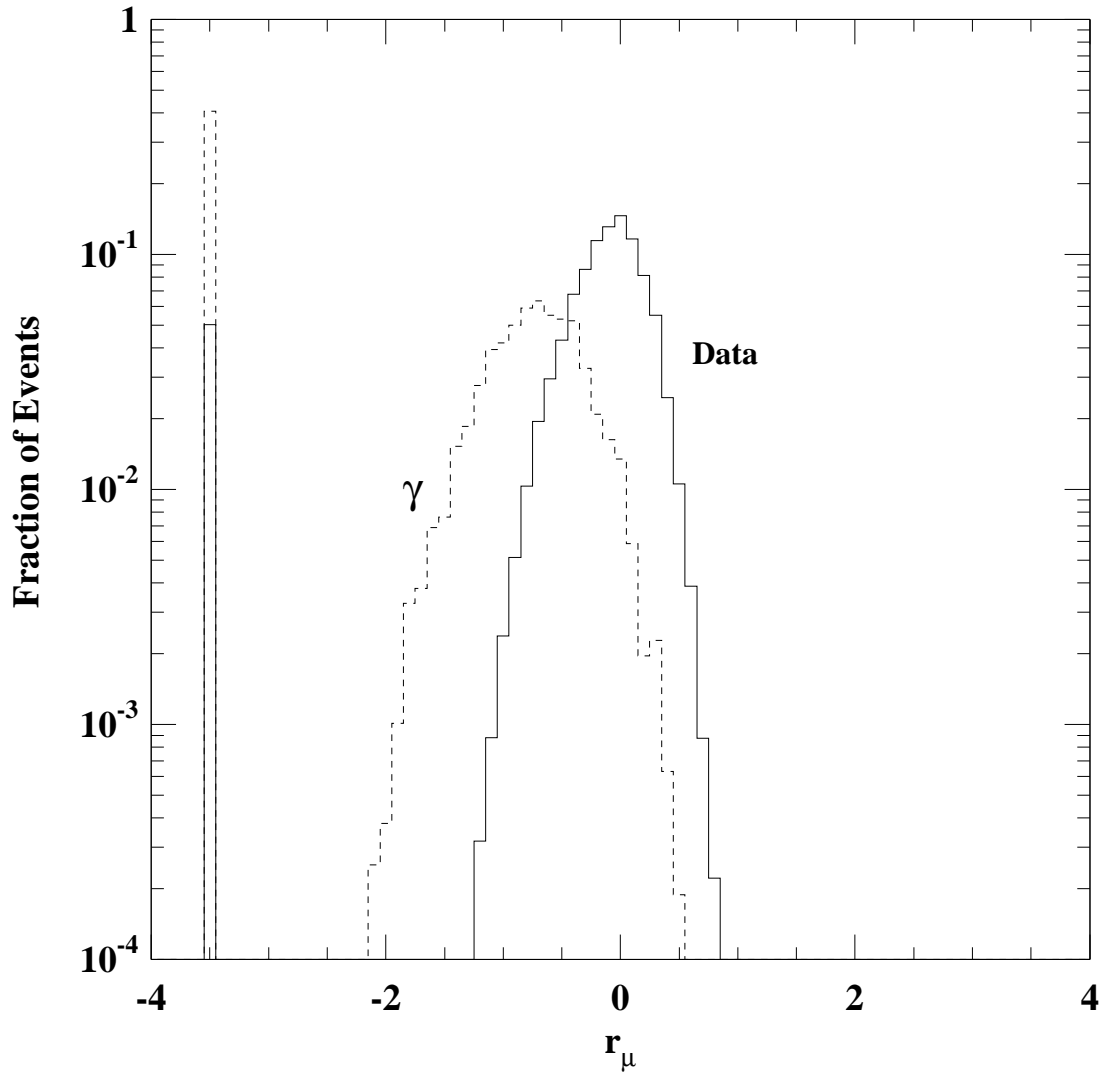


Figure 6: Distributions of the relative muon content, r_μ , for cosmic ray data events (solid) and simulated gamma-ray events (dashed). The quantity r_μ is defined in the text. Events with zero muons are assigned a value of $r_\mu = -3.5$. The gamma-ray simulation uses an input energy spectrum with the same power law spectral index as the cosmic ray data.

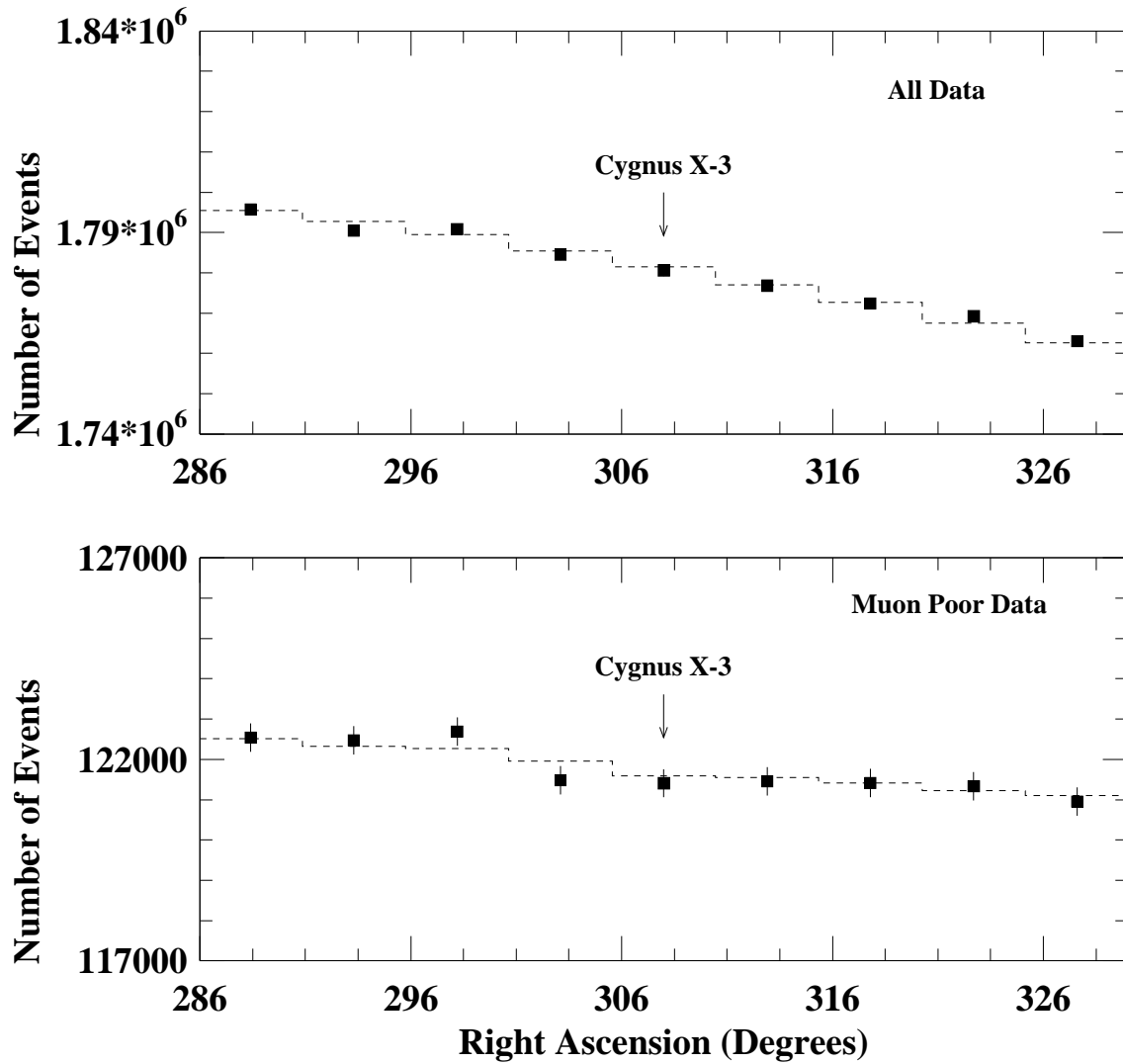


Figure 7: Scans in right ascension for a band of constant declination centered on Cygnus X-3, at a median energy of 115 TeV. The data points correspond to the numbers of events observed in each bin; the dashed histogram is the expected background level. Top plot shows the all-data sample; bottom plot shows the muon-poor sample. Note that the scale on the vertical axis has been highly expanded and zero-suppressed.

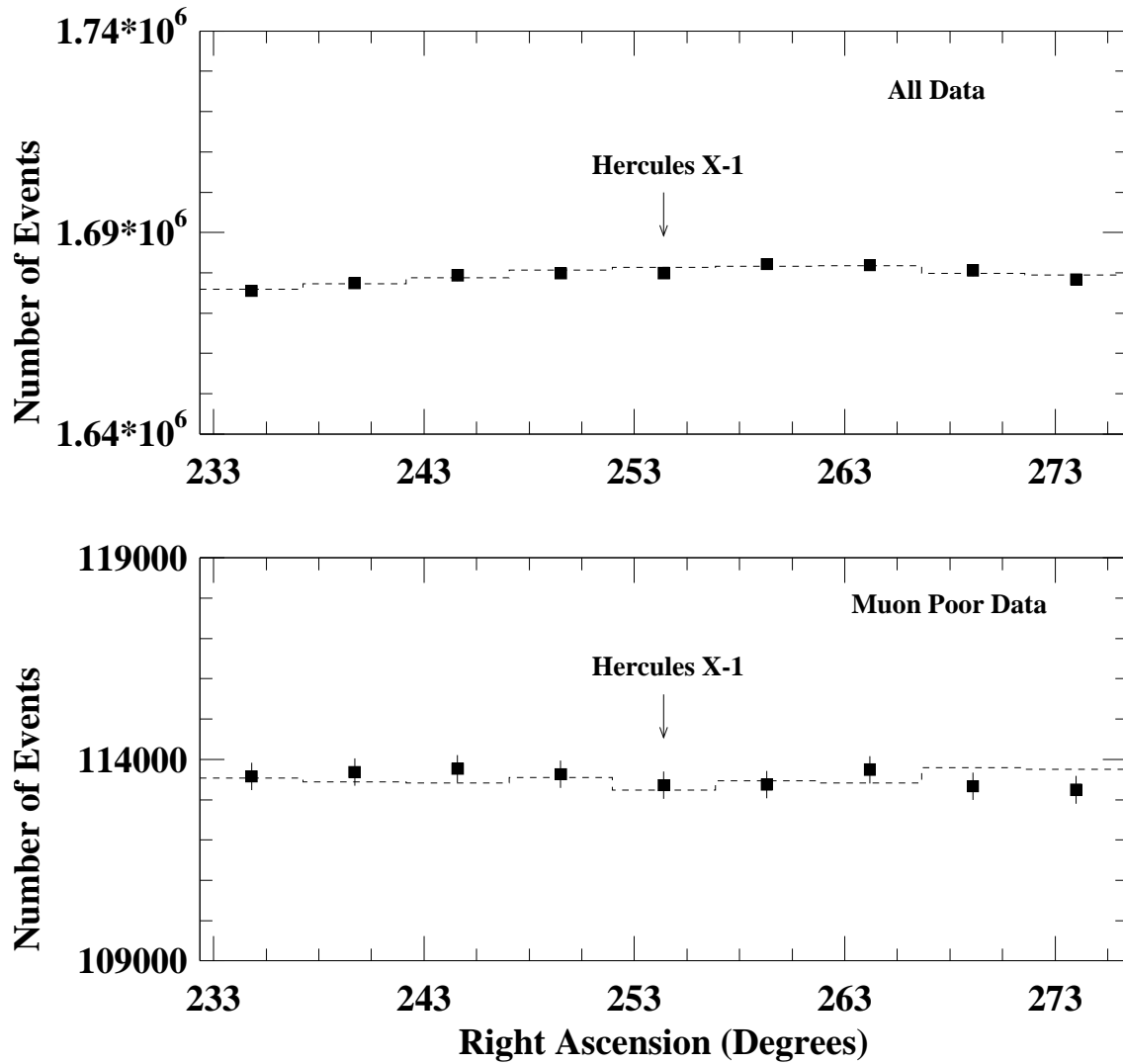


Figure 8: Scans in right ascension for a band of constant declination centered on Hercules X-1, at a median energy of 115 TeV. The data points correspond to the numbers of events observed in each bin; the dashed histogram is the expected background level. Top plot shows the all-data sample; bottom plot shows the muon-poor sample. Note that the scale on the vertical axis has been highly expanded and zero-suppressed.

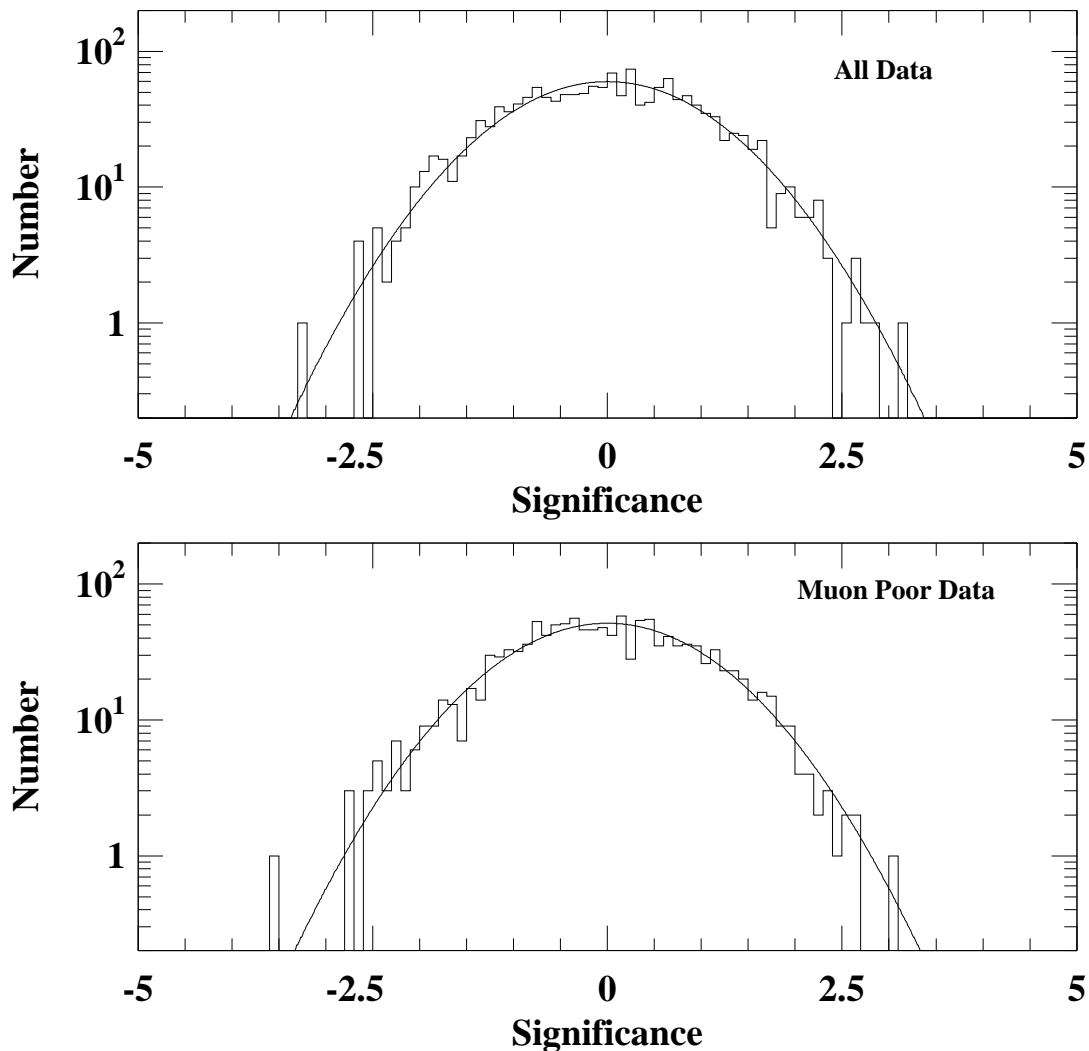


Figure 9: Distribution of transit significances for Cygnus X-3 for the all-data (top) and muon-poor (bottom) samples. The curves are unit-width Gaussian distributions with zero mean. For comparison, the fitted mean (standard deviation) of the all-data sample is -0.040 ± 0.031 (1.011 ± 0.021) and the fitted mean (standard deviation) of the muon-poor sample is -0.011 ± 0.032 (0.992 ± 0.022).

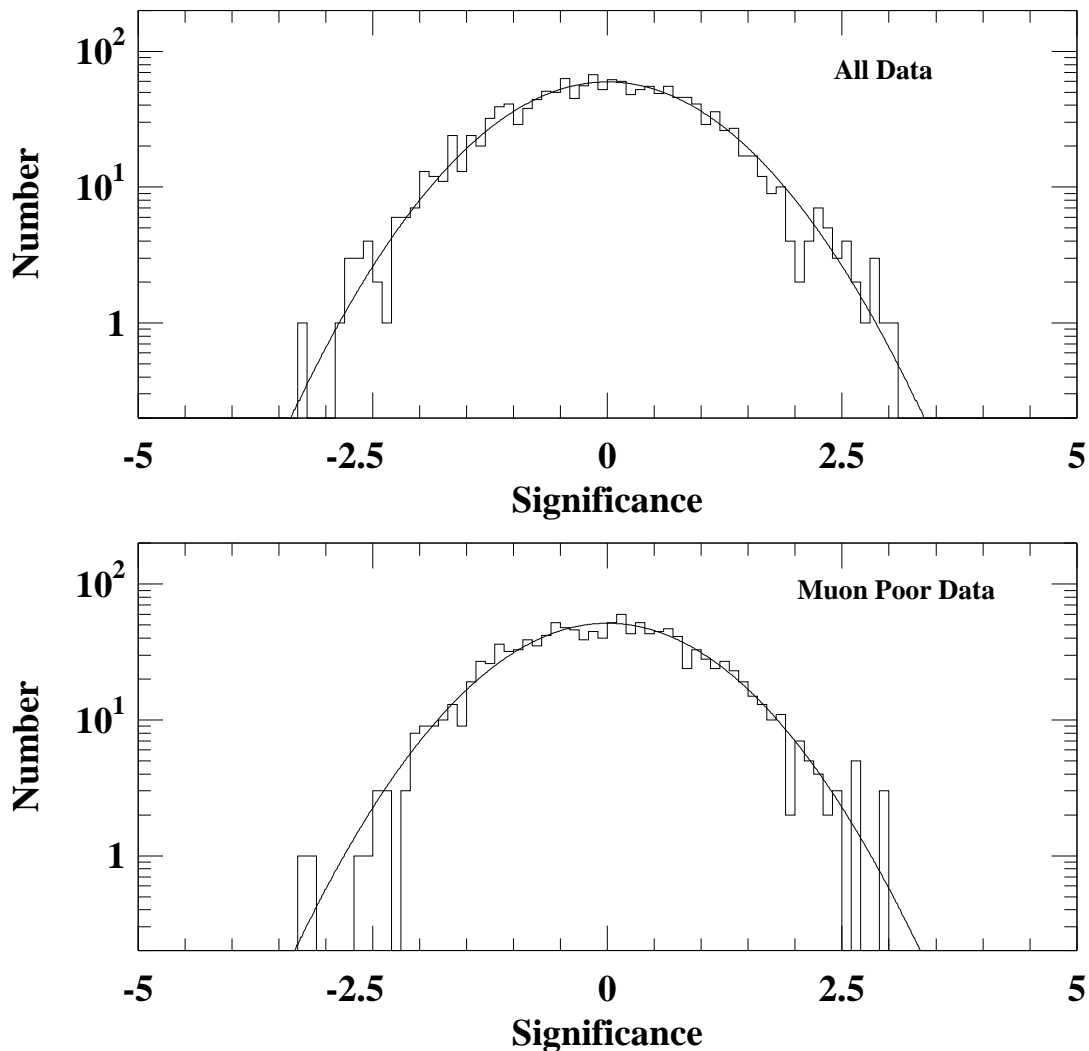


Figure 10: Distribution of transit significances for Hercules X-3 for the all-data (top) and muon-poor (bottom) samples. The curves are unit-width Gaussian distributions with zero mean. For comparison, the fitted mean (standard deviation) of the all-data sample is -0.032 ± 0.031 (0.973 ± 0.020) and the fitted mean (standard deviation) of the muon-poor sample is 0.030 ± 0.033 (0.976 ± 0.022).

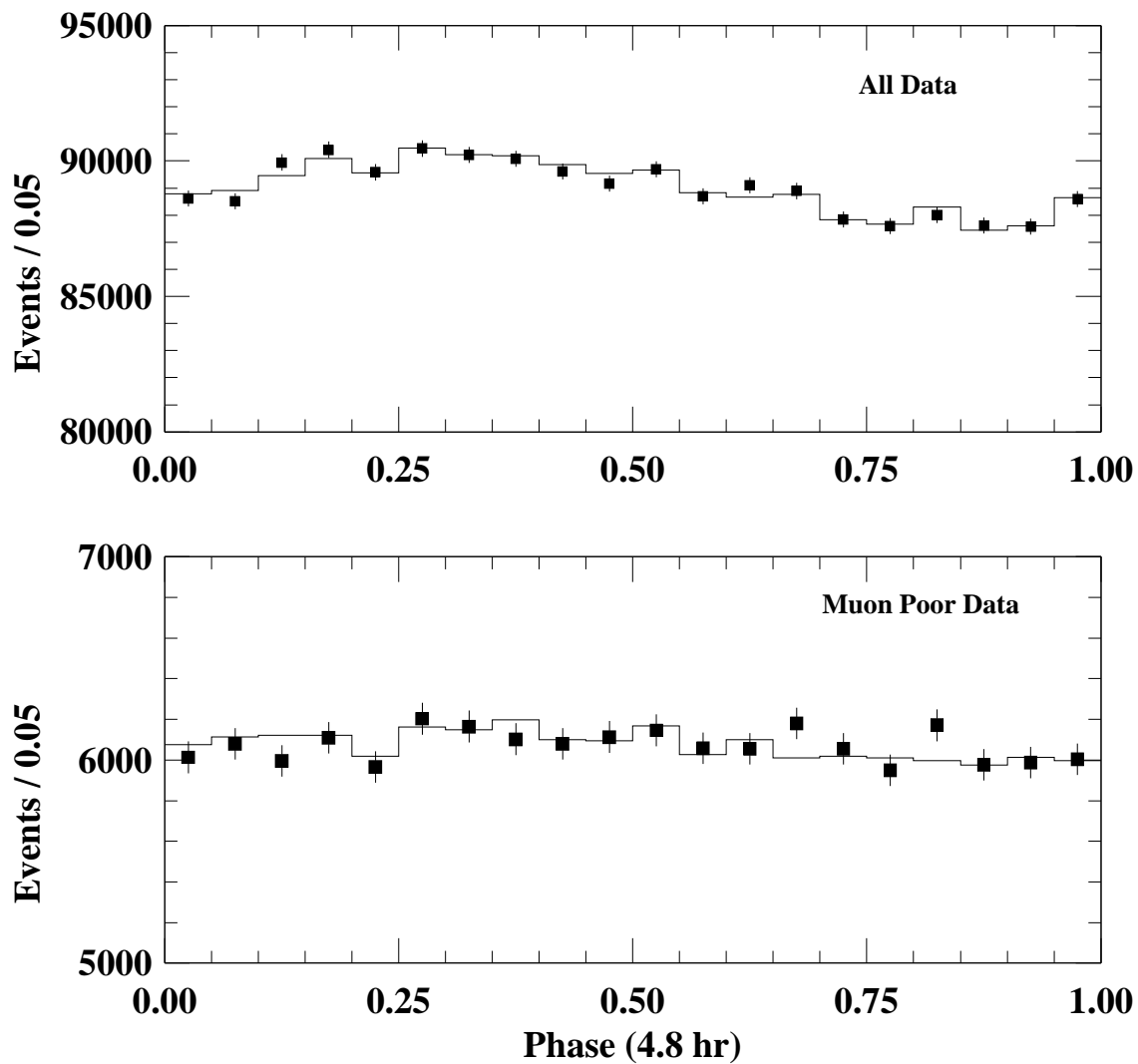


Figure 11: Phase distributions for events from Cygnus X-3 based on the 4.8 hr X-ray periodicity. Data points show the numbers of on-source events in each phase bin for the all-data (top) and muon-poor (bottom) samples. Histograms show the expected background levels.

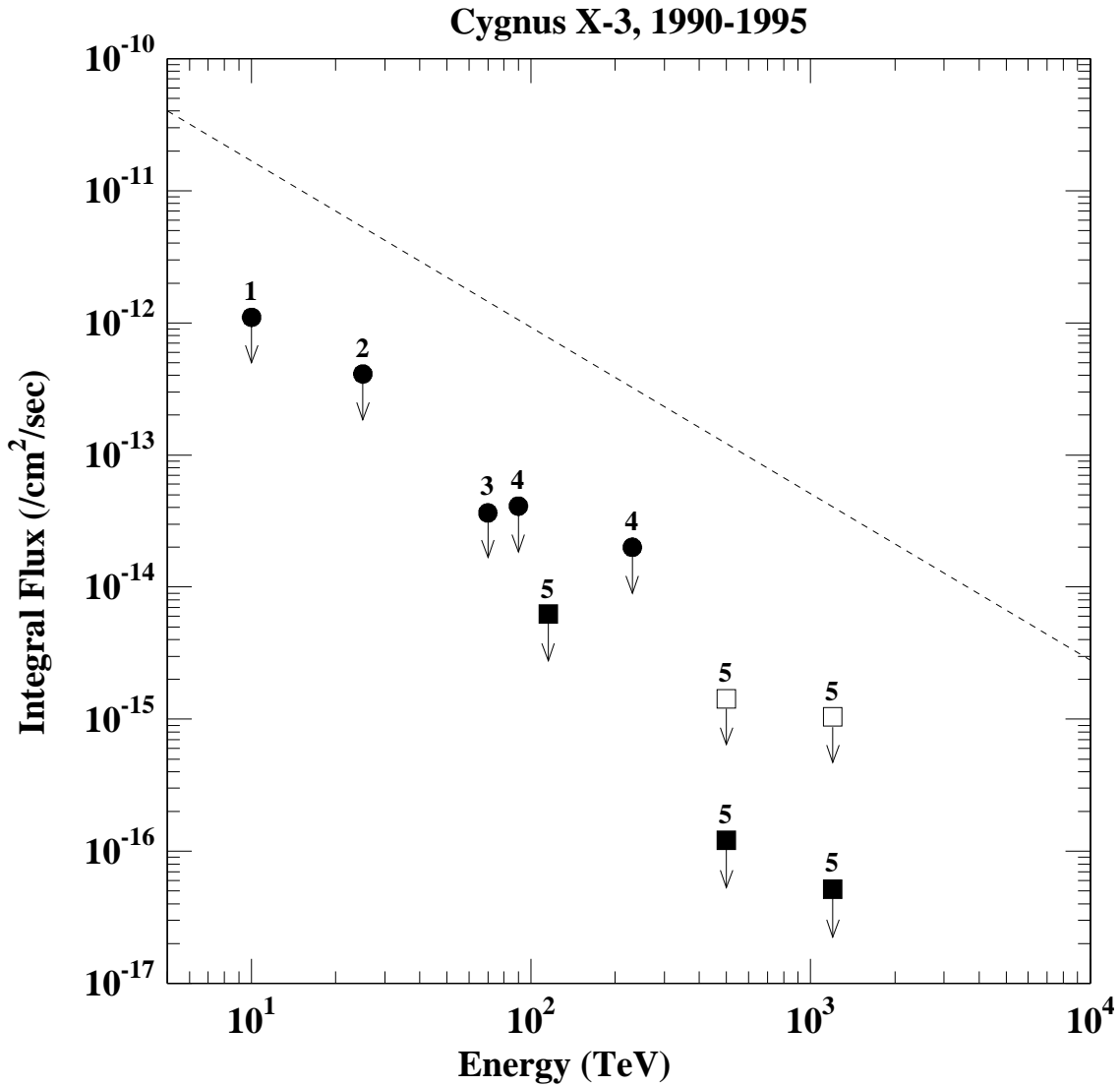


Figure 12: Flux limits reported between 1990 and 1995 on the steady emission of particles from Cygnus X-3. The squares (5) represent the results of this work. Open squares indicate limits on the emission of any neutral particle that creates air showers. Filled squares indicate limits on the emission of gamma-rays. The circles (1-4) represent results from other experiments: 1. Tibet [92], 2. HEGRA [95], 3. CYGNUS [93], and 4. EAS-TOP [94]. The dashed curve is the approximate power law fit to early results (reproduced from Figure 1).

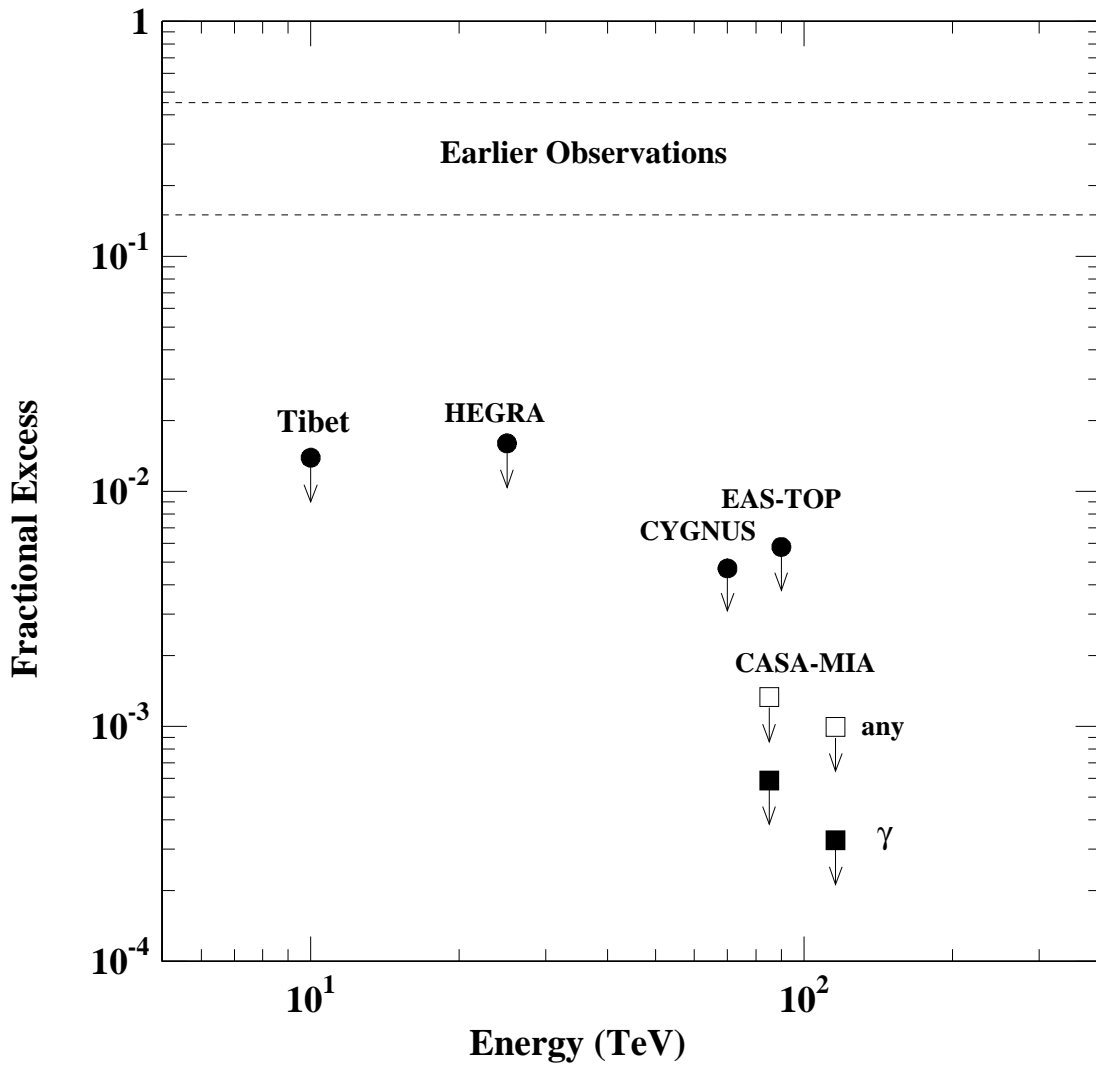


Figure 13: Limits reported between 1990 and 1995 on the fractional excess of gamma-rays from Cygnus X-3 relative to the cosmic ray background. The squares represent the results of this work. Open squares indicate limits on the emission of any neutral particle that creates air showers. Filled squares indicate limits on the emission of gamma-rays. The circles represent results from other experiments: Tibet [92], HEGRA [95], CYGNUS [93], and EAS-TOP [94]. The dashed lines indicate the range of fractional excess values corresponding to the fluxes reported by earlier experiments.

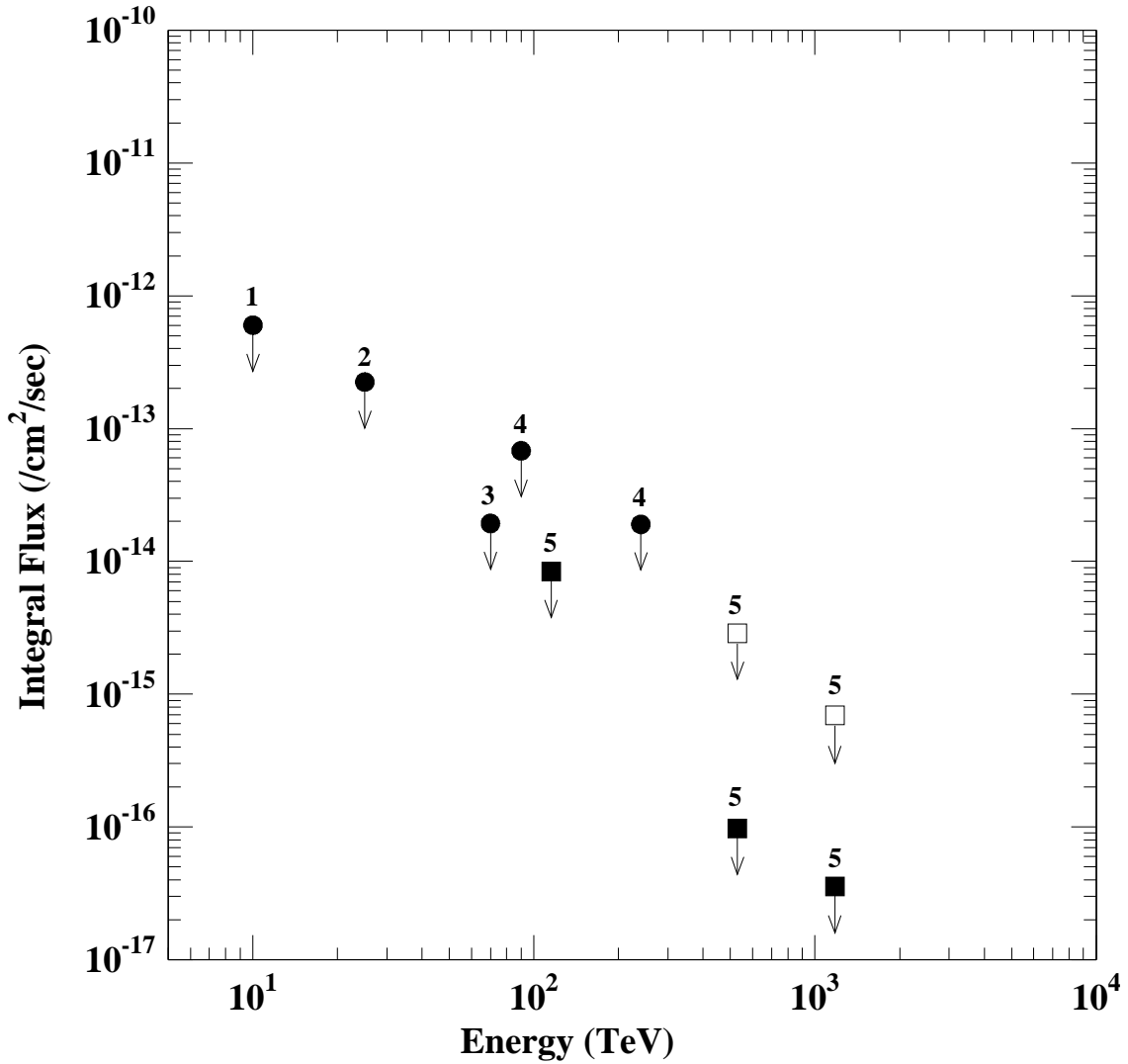


Figure 14: Flux limits reported between 1990 and 1995 on the steady emission of particles from Hercules X-1. The squares (5) represent the results of this work. Open squares indicate limits on the emission of any neutral particle that creates air showers. Filled squares indicate limits on the emission of gamma-rays. The circles (1-4) represent results from other experiments: 1. Tibet [92], 2. HEGRA [95], 3. CYGNUS [93], and 4. EAS-TOP [94].

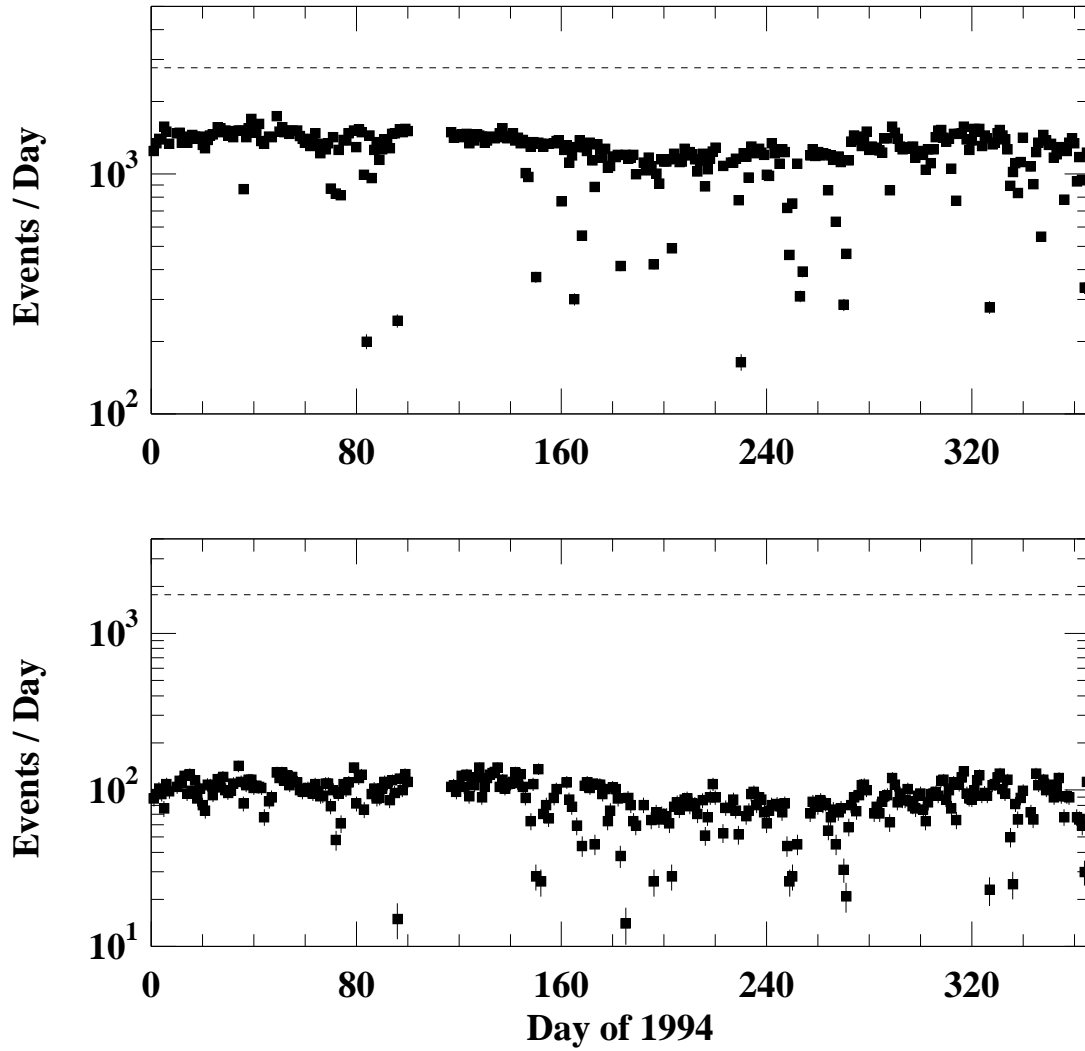


Figure 15: Daily event totals in 1994 for showers recorded by CASA-MIA from the direction of Hercules X-1 for the all-data (top) and muon-poor (bottom) samples. The dashed lines indicate the expected numbers of events for gamma-ray fluxes comparable to those seen in 1986 [60]. The gaps in the distribution indicate those periods in which the experiment recorded no usable data from Hercules X-1.